저작자표시-비영리-변경금지 2.0 대한민국

이용자는 아래의 조건을 따르는 경우에 한하여 자유롭게

- 이 저작물을 복제, 배포, 전송, 전시, 공연 및 방송할 수 있습니다.

다음과 같은 조건을 따라야 합니다:

저작자표시. 귀하는 원저작자를 표시하여야 합니다.

비영리. 귀하는 이 저작물을 영리 목적으로 이용할 수 없습니다.

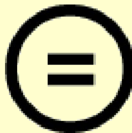

변경금지. 귀하는 이 저작물을 개작, 변형 또는 가공할 수 없습니다.

- 귀하는, 이 저작물의 재이용이나 배포의 경우, 이 저작물에 적용된 이용허락조건을 명확하게 나타내어야 합니다.
- 저작권자로부터 별도의 허가를 받으면 이러한 조건들은 적용되지 않습니다.

저작권법에 따른 이용자의 권리는 위의 내용에 의하여 영향을 받지 않습니다.

이것은 이용허락규약(Legal Code)을 이해하기 쉽게 요약한 것입니다.

Disclaimer

dCollection

[UCI]I804:24011-200000264267

2014年 2月 碩士學位論文 Characteristics of CIS Thin Films by RTA Process after Co-Sputtering 鄭東鉉

2014年 2月

碩士學位 論文

Characteristics of CIS Thin Films by RTA Process after Co-Sputtering

朝鮮大學校 大學院

電氣工學科

鄭 東 鉉

Characteristics of CIS Thin Films by RTA Process after Co-Sputtering

동시스퍼터링 증착 후 급속열처리 CIS 박막 특성

2014年 2月 25日

朝鮮大學校 大學院

電氣工學科

鄭 東 鉉

Characteristics of CIS Thin Films by RTA Process after Co-Sputtering

指導敎授　李 愚 宣

이 論文을 工學碩士學位 申請 論文으로 提出함.

2013年 10月

朝鮮大學校 大學院

電氣工學科

鄭 東 鉉

鄭東鉉의 碩士學位論文을 認准함

委員長 朝鮮大學校 教授 曺 錦 培 印

委 員 朝鮮大學校 教授 金 南 勳 印

委 員 朝鮮大學校 教授 李 愚 宣 印

2013年 11月

朝鮮大學校 大學院

Contents

Abstract

Ⅰ. Introduction ········· 1

Ⅱ. Theoretical Background ········· 4

A. Photovoltaic Devices ········· 4

B. CIS Thin-Film Solar Cells ········· 9

C. Fabrication of CIS Thin-Film Solar Cells ········· 12

D. Characterization of Thin Films ········· 15

Ⅲ. Experimental Details ········· 18

A. Preparation of Thin Films ········· 18

B. Rapid Thermal Annealing for Thin Films ········· 20

C. Characterization of Thin Films ········· 21

Ⅳ. Results and Discussion ········· 22

Ⅴ. Conclusion ········· 50

References ········· 52

Acknowledgement

List of Table

Table. 1 Process conditions in co-sputtering for CIS thin films ··················19

List of Figures

Fig. 1 Concept of Si solar cell and electron flow in solar cell ··············· 4

Fig. 2 Comparison of the electronic band structures of metals, semiconductors and insulators ··············· 5

Fig. 3 A p-n junction in thermal equilibrium with zero bias voltage applied ··············· 7

Fig. 4 Chalcopyrite unit cell structure: Red is Cu, blue is Se and yellow is In/Ga ··············· 9

Fig. 5 Schematic arrangement and band alignment for a $CuInSe_2$ thin film solar cell with a transparent front contact ··············· 10

Fig. 6 Three-stage co-evaporation process of NREL ··············· 12

Fig. 7 Schematic for metallic layers followed by selenization process ··············· 13

Fig. 8 Proposed method for preparing CIS thin films without an additional H_2Se or Se vapor in RTA process ··············· 14

Fig. 9 Photograph of co-sputtering equipment (IDT Engineering Co.) ········· 18

Fig. 10 Photograph of rapid thermal annealing (Modular Process Technology Co., RTP-600S) ··············· 20

Fig. 11. Photographs of HR UV-VIS-NIR spectrophotometer and Hall effect measurement system ··············· 21

Fig. 12 XRD patterns of the as-deposited CIS thin films at the various sputtering powers of 10, 15, 20, 25, and 30 W for In target at the fixed power of 65 W for $CuSe_2$ target with a change of co-sputtering times for 49, 34, 25, 23 and 21 minute, respectively ··············· 24

Fig. 13 XRD patterns of the RTA-treated (400℃ for 10 seconds in N_2 gas ambient) CIS thin films at the various sputtering powers of 10, 15, 20, 25, and 30 W for In target at the fixed power of 65 W for $CuSe_2$ target with a change of co-sputtering times for 49, 34, 25, 23 and 21 minute, respectively ··············· 25

Fig. 14 Distortion parameter η and inter-planar spacing $d_{(112)}$ of the RTA-treated (400℃ for 10 seconds in N_2 gas ambient) CIS thin films at the various sputtering powers of

10, 15, 20, 25, and 30 W for In target at the fixed power of 65 W for $CuSe_2$ target with a change of co-sputtering times for 49, 34, 25, 23 and 21 minute, respectively 29

Fig. 15 Atomic percentage of the as-deposited and RTA-treated (400℃ for 10 seconds in N_2 gas ambient) CIS thin films at the various sputtering powers of 10, 15, 20, 25, and 30 W for In target at the fixed power of 65 W for $CuSe_2$ target with a change of co-sputtering times for 49, 34, 25, 23 and 21 minute, respectively 30

Fig. 16 Deviation parameters of $\Delta m = [Cu]/[In] -1$ and $\Delta s = 2[Se]/([Cu]+3[In]) -1$ from the chemical compositions of the RTA-treated (400℃ for 10 seconds in N_2 gas ambient) CIS thin films at the various sputtering powers of 10, 15, 20, 25, and 30 W for In target at the fixed power of 65 W for $CuSe_2$ target with a change of co-sputtering times for 49, 34, 25, 23 and 21 minute, respectively 31

Fig. 17 Optical transmittance of the as-deposited CIS thin films at the various sputtering powers of 10, 15, 20, 25, and 30 W for In target at the fixed power of 65 W for $CuSe_2$ target with a change of co-sputtering times for 49, 34, 25, 23 and 21 minute, respectively 35

Fig. 18 Optical transmittance of the RTA-treated (400℃ for 10 seconds in N_2 gas ambient) CIS thin films at the various sputtering powers of 10, 15, 20, 25, and 30 W for In target at the fixed power of 65 W for $CuSe_2$ target with a change of co-sputtering times for 49, 34, 25, 23 and 21 minute, respectively 36

Fig. 19 The calculated band gap energies (E_g) of the RTA-treated (400℃ for 10 seconds in N_2 gas ambient) CIS thin films at the various sputtering powers of 10, 15, 20, 25, and 30 W for In target at the fixed power of 65 W for $CuSe_2$ target with a change of co-sputtering times for 49, 34, 25, 23 and 21 minute, respectively 37

Fig. 20 Absorption coefficient (α) spectra of the as-deposited CIS thin films at the various sputtering powers of 10, 15, 20, 25, and 30 W for In target at the fixed power of 65 W for $CuSe_2$ target with a change of co-sputtering times for 49, 34, 25, 23 and 21 minute, respectively 41

Fig. 21 Absorption coefficient (α) spectra of the RTA-treated (400℃ for 10 seconds in N_2 gas ambient) CIS thin films at the various sputtering powers of 10, 15, 20, 25, and 30 W for In target at the fixed power of 65 W for $CuSe_2$ target with a change of co-sputtering times for 49, 34, 25, 23 and 21 minute, respectively ········ 42

Fig. 22 Average absorbance in the range of 400 -1500 nm of (a) the as-deposited and (b) RTA-treated (400℃ for 10 seconds in N_2 gas ambient) CIS thin films at the various sputtering powers of 10, 15, 20, 25, and 30 W for In target at the fixed power of 65 W for $CuSe_2$ target with a change of co-sputtering times for 49, 34, 25, 23 and 21 minute, respectively ········ 43

Fig. 23 Tauc plot of $(\alpha h\upsilon)^2$ vs. the photon energy ($h\upsilon$) for the as-deposited CIS thin films at the various sputtering powers of 10, 15, 20, 25, and 30 W for In target at the fixed power of 65 W for $CuSe_2$ target with a change of co-sputtering times for 49, 34, 25, 23 and 21 minute, respectively ········ 44

Fig. 24 Tauc plot of $(\alpha h\upsilon)^2$ vs. the photon energy ($h\upsilon$) for the RTA-treated (400℃ for 10 seconds in N_2 gas ambient) CIS thin films at the various sputtering powers of 10, 15, 20, 25, and 30 W for In target at the fixed power of 65 W for $CuSe_2$ target with a change of co-sputtering times for 49, 34, 25, 23 and 21 minute, respectively ········ 45

Fig. 25 Hall effect measurements: Resistivity (ρ), carrier concentration (n), and carrier mobility (μ) of the as-deposited CIS thin films at the various sputtering powers of 10, 15, 20, 25, and 30 W for In target at the fixed power of 65 W for $CuSe_2$ target with a change of co-sputtering times for 49, 34, 25, 23 and 21 minute, respectively ········ 48

Fig. 26 Hall effect measurements: Resistivity (ρ), carrier concentration (n), and carrier mobility (μ) of the RTA-treated (400℃ for 10 seconds in N_2 gas ambient) CIS thin films at the various sputtering powers of 10, 15, 20, 25, and 30 W for In target at the fixed power of 65 W for $CuSe_2$ target with a change of co-sputtering times for 49, 34, 25, 23 and 21 minute, respectively ········ 49

ABSTRACT

동시스퍼터링 증착 후 급속열처리 CIS 박막 특성

Chung, Dong Hyun
Advisor : Prof. Lee, Woo-Sun, Ph D.
Department of Electrical Engineering
Graduate School of Chosun University

높은 광흡수계수 및 1.04 eV의 적합한 밴드갭 에너지를 갖는 이유로 $CuInSe_2$ (CIS) 박막이 이종접합 박막 태양전지 응용에서 광흡수층으로 사용되어지고 있다. CIS 박막 태양전지는 최근 20%를 상회하는 변환효율을 달성함으로써 신재생에너지 산업의 가장 유력한 광기전력 소자로 고려되어지고 있다. CIS 박막은 일반적으로 동시진공증착(co-evaporation) 방법으로 제조되어지는데, 필수적인 셀렌화(selenization) 공정을 위하여 셀렌(selenium) 가스를 사용하게 되어 고가의 복잡한 장비가 필요하며 각각의 원소들에 대한 증착률의 정확한 제어가 어려운 대량 생산에의 심각한 문제가 있다.

본 논문에서는 마그네트론 동시스퍼터링(co-sputtering) 방법으로 이셀렌구리($CuSe_2$) 및 인듐(In) 타겟을 사용하여 증착하고 질소(N_2) 가스 분위기에서 급속열처리(rapid thermal annealing, RTA) 공정을 적용하여 CIS 박막을 제조하는 방법을 최초로 제안하였다.

CIS 박막 내의 셀렌(Se)의 조성비는 셀렌의 휘발 특성에 기인하여 고온

및 장시간 열처리 공정을 적용하였을 시에 고효율 태양전지 소자에서 요구하는 수준 이하로 제작되어 진다. 따라서 급속열처리 공정을 적용하여 비교적 저온에서 짧은 시간동안 열처리를 수행함으로써 셀렌의 정확한 조성비 제어를 가능하게 하여 추가적인 셀렌 포함 가스의 주입 없이 열처리 공정을 할 수 있을 것으로 기대된다. 또한 동시스퍼터링 공정에서 인듐 타겟의 스퍼터링 파워를 조정함으로써 CIS 박막의 화학량론적인 조성비를 제어할 수 있다.

이상의 공정을 통하여 제조한 박막에서 CIS 칼코파이라이트(chalcopyrite) 결정구조가 (112) (220)/(204) (312)/(116) 면을 따라서 성장하였음을 X-ray 회절(X-ray diffraction) 분석을 통해서 확인할 수 있었다. 급속열처리 공정을 수행한 CIS 박막의 화학조성 분석에서 다소간 Se의 휘발이 발생함을 확인하였으며, 인듐에 대한 스퍼터링 파워가 상대적으로 낮았을 때에는 구리(Cu)-초과 및 셀렌-부족 박막 및 상대적으로 높았을 때에는 구리-초과 및 셀렌-과잉 박막이 형성되었다.

급속열처리 공정을 수행한 CIS 박막의 광학적 특성을 조사하였을 때에 밴드갭 에너지(E_g)는 인듐의 조성비에 따라서 0.98~1.49eV으로 변화하였고, 이는 구리/인듐 조성비 편차인 Δm의 경향성과 정확히 반비례하는 결과임을 확인할 수 있었다. 급속열처리 공정을 수행한 CIS 박막의 평균 흡광도(absorbance)는 1.24로써 이는 가시광~근적외선(400~1500nm)의 입사광 91.7%가 약 500nm 두께의 CIS 박막 광흡수층에 흡수됨을 나타낸다.

캐리어 농도는 급속열처리 공정을 수행한 CIS 박막 모두에서 p형 전도특성과 10^{17} - 10^{21} cm^{-3} 수준을 나타내었고, 비저항은 10^{-3} - 10^{1} Ω-cm로써 구리-초과 조성 및 높은 캐리어 농도에 기인하여 기존에 보고된 수준보다 우수한 특성을 나타내었다.

Ⅰ. Introduction

When the photovoltaic-industry was deemed to be a strategic industry as a sustainable energy source which could substitute for fossil fuels, copper indium diselenide ($CuInSe_2$, CIS) thin films based solar cells had already been entering into commercial mass-production on a 100 MW/year scale [1]. Compound I-III-VI_2 semiconductors have been used for many applications such as infrared and X-ray imaging systems, optical devices for telecommunications, and solar cells [2,3]. The compound I-III-VI_2 semiconductor CIS thin film is one of the primary candidates in the field of photovoltaic energy conversion due to its specific advantages.

Recently, considerable attention has been paid to thin-film solar cells including polycrystalline CIS thin films with a chalcopyrite lattice structure as an absorber layer owing to its suitable optical absorption (> 10^5 cm^{-1}), long-term electrothermal stability, high tolerance to defects, no toxic or hazardous pollutants, such as arsenic and cadmium, and an appropriate band gap (E_g = 1.04 eV) [4,5]. The highest conversion efficiency up to 20% has been achieved in heterostructured CIS solar cells, which is approaching the highest efficiency of conventional polycrystalline silicon solar cells [6,7].

A co-evaporation and post-selenization process is widely employed for achieving high conversion efficiency but this conventional method has several drawbacks impeding industrial production, such as process complexity, expensive equipment, slow deposition rate and poor reproducibility [8].

Against the conventional manufacturing processes, the selenization of sputtered I-III-VI_2 precursors using H_2Se vapor was proposed as a suitable method for preparing CIS thin films at low cost [9]. On the other hand, critical problems in the selenization process still remain, such as highly

toxic H_2Se, slow reaction rate and poor adhesion with back contact [4].

Therefore, a non-selenization process is needed to prepare CIS thin films. Few studies have been performed. AVANCIS GmbH and Co. KG formed an elemental precursor film by DC-magnetron sputtering of I-III-VI_2 compound and the thermal evaporation of Se followed by rapid thermal annealing (RTA) in a sulfur containing ambient [10,11]. Jheng *et al.* prepared I-III-VI_2 thin films by co-sputtering with Cu-Ga alloy and In-Se alloy targets before a two-step annealing process without an additional selenium source under vacuum [4].

A novel method was proposed for preparing a chalcopyrite I-III-VI_2 thin film without a selenization process by RF magnetron sputtering with In, Ga and $CuSe_2$ alloy targets in the previous study [12]. Copper (Cu) chalcogenide compounds have been widely used in electronics, optoelectronics and photovoltaics because of their superior performance in areas, such as Shottky diodes, super ionic conductors, photodetectors, electro-conductive electrodes and solar cells [13,14]. Copper selenide is a chalcogenide compound with semiconducting behavior that can show a wide deviation from stoichiometry: $CuSe_2$, one of the copper selinides, generally has a cubic and orthorhombic structure that melts incongruently to CuSe and a Se-rich liquid at 347℃ [15,16]. This process with $CuSe_2$ has many advantages including simplicity without an additional selenization process, large-area manufacturing for mass production, and excellent electrical and optical properties [12]. Another merit of this novel method is the ease of adjusting chemical composition ratio in I-III-VI_2 thin films.

In this thesis, influences of the chemical composition and the post-deposition annealing treatment with RTA on the properties of the CIS thin films were investigated. The co-sputtering process for I-III-VI_2 precursors with $CuSe_2$ target was firstly proposed instead of the previously-reported multi-stack structure with a gradual deposition in DC-magnetron sputtering. The structure behaviors of CIS thin films were

analyzed using X-ray diffraction (XRD) as a function of the co-sputtering power for controlling the chemical composition ratio in CIS thin films. The effect of chemical composition ration in CIS thin films was examined with RTA treatment by analyzing the electrical and optical properties including the optical transmittance, absorption coefficient, mean absorbance, carrier concentration and resistivity.

The aim of my thesis is to develop the novel fabrication process for CIS thin films with simplicity, low-cost, mass-production, no toxic or hazardous pollutants and excellent thin-film properties. For this purpose, some experiments and analyses were used. Chapter II contains description of theoretical background with the prior literatures, which used for the experimental demonstration in Chapter III. Results of the preparations and analyses are described in Chapter IV. Finally, some conclusions of this thesis are summarized in Chapter V.

Ⅱ. Theoretical Background

A. Photovoltaic Devices[1)]

Photovoltaic devices (solar cells) are devices that convert light energy into electrical energy. The light-absorber-layer in the solid state semiconductor solar cells can either be a single crystal, polycrystalline or amorphous semiconductor. Silicon (Si) is the most widely used material for solar cells. Other material, such as cadmium telluride (CdTe) and copper indium (gallium) selenide (CI(G)S) have received more concentration during recent years.

These materials are mainly prepared as polycrystalline thin-films. There is an advantage of these materials in comparison to Si in the good light absorption properties which reduces the required layer thickness from about a hundred μm down to only a few or sub-μm. This advantage makes them potentially cheaper to produce if an efficient fabrication method is applied.

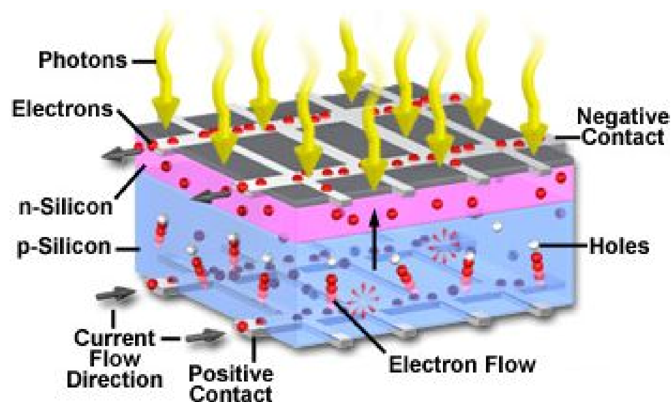

Fig. 1 Concept of Si solar cell and electron flow in solar cell [17]

---

1) This chapter is referred and summarized in http://www.haverford.edu/kinsc/boe/dssc.

A semiconductor solar cell is essentially a pn-junction diode fabricated from suitable light-absorbing materials. Under illumination, photons with energies higher than the band gap of the material are absorbed by electrons in the valence band. These electrons are excited to the conduction band and thereby excess electron-hole pairs are generated. These pairs may be separated by the built-in field if the carriers are generated either within the depletion region or close enough to be able to diffuse into it. The separated holes and electrons create a current from the n-doped side towards the p-doped side of the junction.

Semiconductors have distinct bands of electron states, the so called valence and conduction bands. These are separated by a forbidden gap of energies, the band gap, where no electron states exists for the ideal crystalline material. Due to the Pauli exclusion principle, two electrons cannot exist in identical energy states. Therefore, at absolute zero, the electrons of a substance will pack down into the lowest energy states available in that substance: The highest energy level occupied by an electron at absolute zero is known as the Fermi level of a substance.

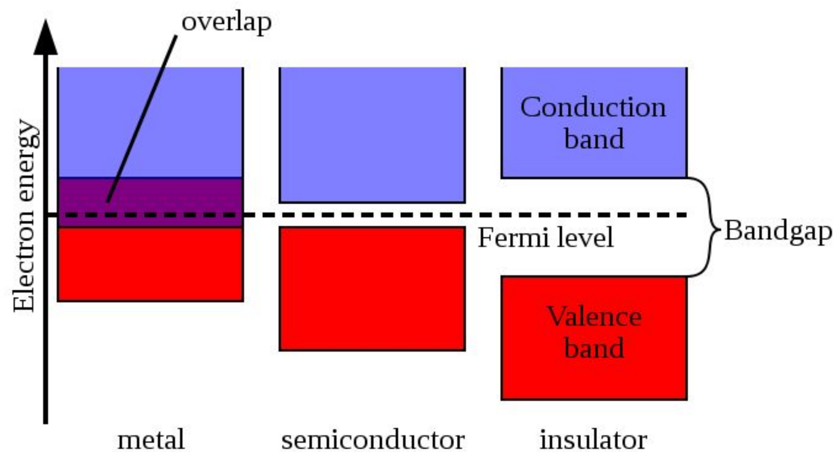

Fig. 2 Comparison of the electronic band structures of metals, semiconductors and insulators [18]

A substance will conduct if, directly above the Fermi level of that substance, there exists a high density of energy states that the electrons of that substance can occupy. That is, electrons can jump up to higher energy levels with little to no energy cost. Essentially, the electrons can move freely between energy levels. When a potential difference is applied to the substance, the energy levels of the atoms of the substance will be changed such that a gradient will be established in the energy levels of the substance - the unoccupied states on the side of the substance with the more positive electric potential will be at a lower energy than the occupied states with the more negative electric potential. For this reason, the electrons will move from the occupied states in the end of the substance with the more negative electric potential to the unoccupied states in the side of the substance with the more positive electric potential. This is allowed because the electrons can move between electric states easily. That is, the electrons are able to flow through the substance; therefore, these substances are called conductors.

In an insulator, there is a large difference in energy between the highest-energy electron-occupied energy level and the lowest-energy unoccupied energy level. This difference is called a band gap. For this reason, it takes a significant amount of energy for electrons to move between energy levels and for this reason, when a potential difference is applied to an insulator, electrons cannot flow as shown in Fig. 2.

A semiconductor is a material with a band gap that is small enough such that electrons can be excited into higher energy states with small amounts of energy. Semiconductors can be used in solar cells when the size of the band gap is equivalent to the energy of the photons emitted by the sun. When solar photons strike these materials, their electrons can be excited into higher energy levels. As the energy levels above the band gap are not filled by the excited electrons, these excited electrons are allowed to flow freely and can be used to create a potential difference as shown in Fig. 2.

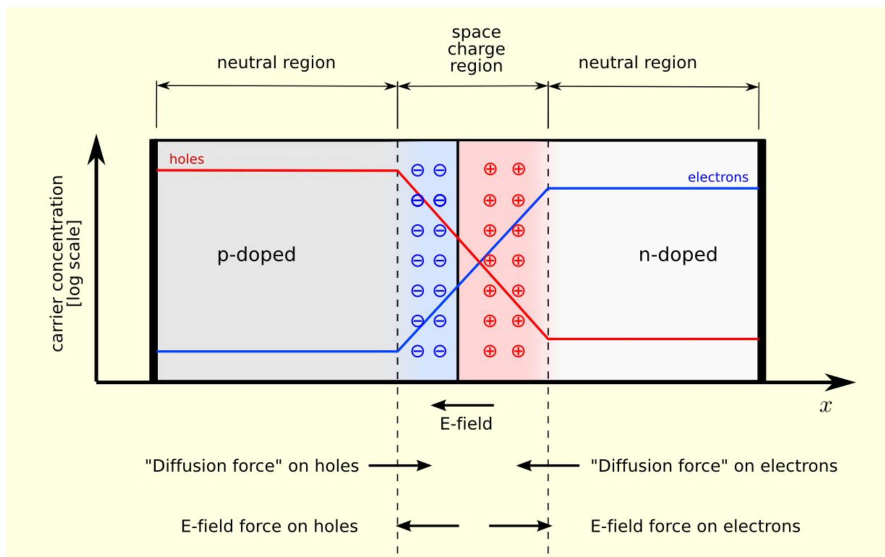

Fig. 3 A p-n junction in thermal equilibrium with zero bias voltage applied [19]

Moving electric charge constitutes a current. This charge must be carried by some particle. There are two main ways of thinking about current flow - in terms of electrons (negative charge carriers) or in terms of holes, which are conceptual particles that indicate the absence of electrons and are considered to be positive charge carriers.

Conventional solar cells are made of Si, a semiconductor material has four electrons in its valence shell - for this reason, it will form bonds to four other Si atoms, forming a lattice. When Si is bonded to four other atoms, none of its electrons are free to move about the lattice. Due to this lack of free electrons, pure Si is an almost-perfect insulator.

Because of this, pure Si is doped for use in solar cells. Other atoms are purposefully introduced into the lattice structure in order to make the solar cell work. When tiny amounts of atoms like phosphorous with five valence electrons are introduced into the lattice, extra electrons are added to the lattice structure, creating n-type Si. On the other hand, when atoms such as boron with only three valence electrons are introduced

into the structure, the structure has an excess of holes, which can be filled with electrons, creating p-type Si.

When a p-type semiconductor is placed in contact with an n-type semiconductor, some of the excess electrons in the n-type material will flow over into the p-type material in order to recombine with some of the extra holes in the p-type material. This does not occur indefinitely, however, when electrons move from the n-type semiconductor into the p-type semiconductor, the atoms of the n-type semiconductor near the p-n junction become positively charged and the atoms of the p-type semiconductor near the p-n junction become negatively charged. This creates an electric field which tends to push electrons into the n-type material. That is, an excess electron in the p-type material would be swept into the n-type material but could not move back across the electric field as shown in Fig. 3. The opposite is true for holes.

So, when a photon from the sun with enough energy to excite one of the electrons in the semiconductor strikes the solar cell, one of the valence electrons in the semiconductor will be excited to a higher energy level, leaving a hole in the old energy level. This hole will tend to be swept towards the p-type material while the electron, which can travel easily between atoms due to the relative lack of other electrons near its energy level will be swept towards the n-type material. The electron will be driven to recombine with its hole; therefore, if the n-type material is connected to the p-type material by an external wire, the electron will travel through the wire from the n-type material to the p-type material, creating moving charge or a current.

In a conventional solar cell, the semiconductor has two main roles - it acts as a source of electrons and provides an electric field in order to separate the charge. Because of this, some of the charge separation is lost when the excited electron recombines with its hole before the two charge carriers have a chance to be separated. This causes a significant decrease in the efficiency of the conventional solar cell.

B. CIS Thin-Film Solar Cells

There are many advantages of using thin films, such as substantial cost advantage, lower consumption of materials, ease of manufacturing large, area devices, fewer processing steps, wider selection of materials, easier integration of monolithic devices and greater tolerance on materials quality [20].

CIS is a direct band gap and is a tetrahedrally bonded semiconductor, with a chalcopyrite crystalline structure as shown in Fig. 4. It has suitable optical absorption (> 10^5 cm^{-1}), long-term electrothermal stability, high tolerance to defects, no toxic or hazardous pollutants, such as arsenic and cadmium, and an appropriate band gap (1.04 eV) as an absorber layer in solar cells. That is, CIS has very strong light absorption and only 1-2 μm of CIS is enough to absorb most of the incident sunlight.

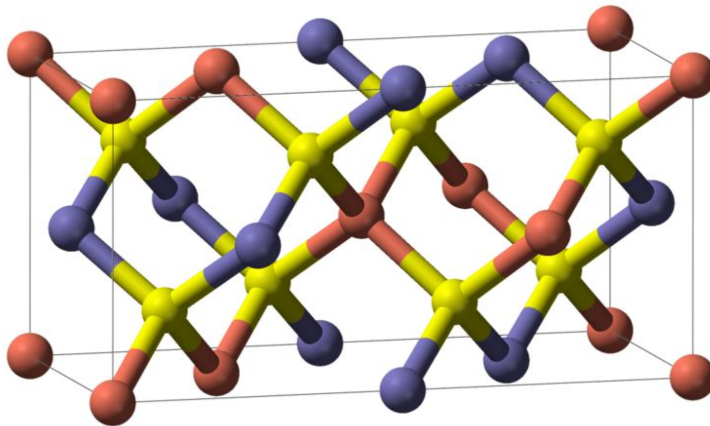

Fig. 4 Chalcopyrite unit cell structure: Red is Cu, blue is Se and yellow is In/Ga [21]

The basic structure of a CIS thin-film solar cell is depicted in Fig. 5. The most common substrate is soda-lime glass of 1-3 mm thickness. This is coated on one side with molybdenum (Mo) that serves as metal back contact. The heterojunction is formed between the semiconductors CIS and zinc oxide (ZnO), separated by a thin layer of cadmium sulfide (CdS) and a layer of intrinsic ZnO. The CIS is doped p-type from intrinsic defects, while the ZnO is doped n-type to a much larger extent through the incorporation of aluminum (Al). This asymmetric doping causes the space-charge region to extend much further into the CIS than into the ZnO. Matched to this are the layer thicknesses and the band gaps of the materials: the wide CIS layer serves as absorber with a band gap 1.04 eV. Absorption is minimized in the upper layers, called window, by the choice of larger band gaps: $E_{g,ZnO}$ = 3.2 eV and $E_{g,CdS}$ = 2.4 eV. The doped ZnO also serves as front contact for current collection.

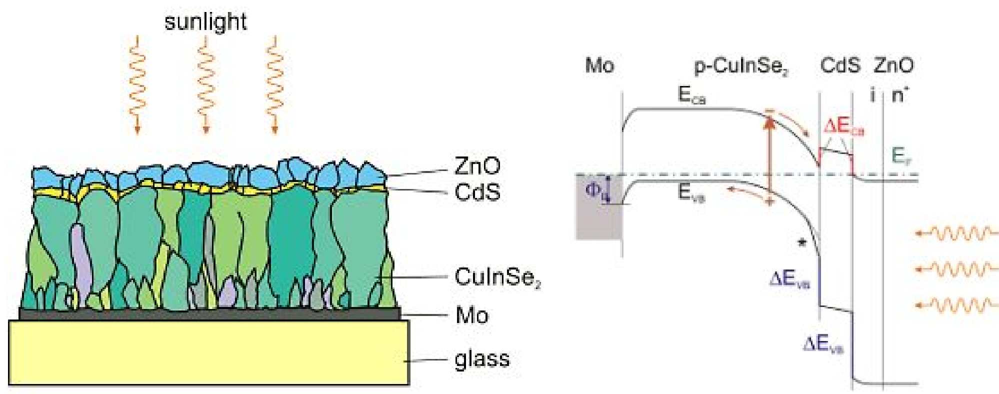

Fig. 5 Schematic arrangement and band alignment for a $CuInSe_2$ thin film solar cell with a transparent front contact [22]

The properties and quality of CIS thin films for optimal performance were influenced by some important factors, such as a incorporation of sodium (Na), an overall Cu deficiency and fabrication method. Cu deficiency increases the majority carrier (hole) concentration by

increasing the number of Cu vacancies which act as electron acceptors. Also, when CIS films are In rich (Cu deficient) the surface layer of the film forms an ordered defect compound (ODC). The ODC is n-type, forming a p-n homojunction in the film at the interface between the α phase and the ODC. Recombination velocity at the CIS/CdS interface is decreased by presence of the homojunction. The drop in interface recombination attributable to ODC formation is demonstrated by experiments which have shown recombination in the bulk of the film is the main loss mechanism in Cu deficient films, while in Cu rich films the main loss is at the CIS/CdS interface.

C. Fabrication of CIS Thin-Film Solar Cells

Co-evaporation is the most prevalent CIS fabrication technique. The Boeing co-evaporation process deposits bi-layers of CI(G)S with different stoichiometries onto a heated substrate and allows them to intermix. The National Renewable Energy Laboratory (NREL) has developed another process which involves three deposition stages. The first stage is co-deposition of In/Ga and Se at relatively low temperature. This is followed by Cu and Se deposited at a higher temperature to allow for diffusion and intermixing of the elements. In the final stage In/Ga and Se are again deposited to ensure the overall In rich (Cu deficient) composition of the film. However, Co-evaporation method also face significant disadvantages including uniformity issues over large areas. Another disadvantage is high growth temperatures (more than 450-500℃ to get CIS chalcopyrite phase) which raise the thermal budget and cost. Additionally, co-evaporation is plagued by low material utilization (deposition on chamber walls instead of the substrate, especially for Se) and expensive vacuum equipment.

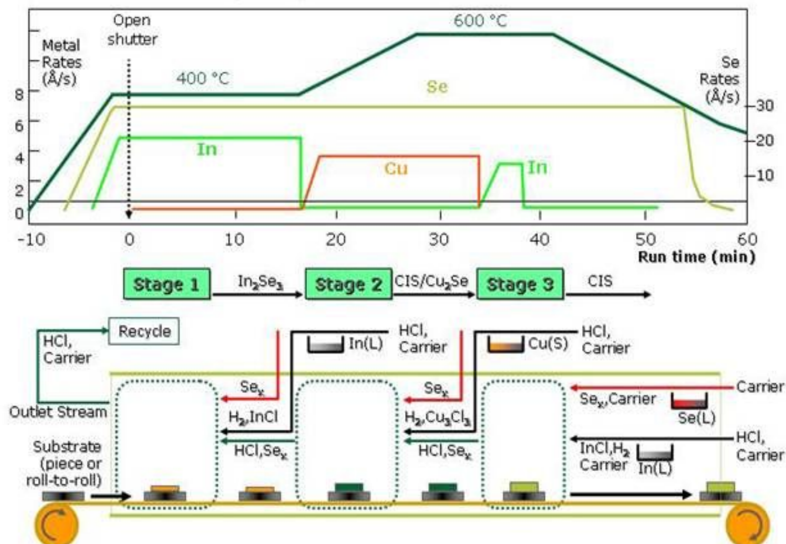

Fig. 6 Three-stage co-evaporation process of NREL [23]

In the selenization method to form CIS absorbers, a metal film of Cu and In is sputtered at or near room temperature and reacted in a Se atmosphere at high temperature as shown in Fig. 7. This process has higher throughput than co-evaporation and compositional uniformity can be more easily achieved.

The Se supply and selenization environment is extremely important in determining the properties and quality of the film produced from precursor layers. When Se is supplied in the gas phase (for example as H_2Se or elemental Se) at high temperatures the Se will become incorporated into the film by absorption and subsequent diffusion. During this step, called chalcogenization, complex interactions occur to form a chalcogenide. These interactions include formation of Cu-In intermetallic alloys, formation of intermediate metal-selenide binary compounds, and phase separation of various stoichiometric CIS compounds. Because of the variety and complexity of the reactions taking place, the properties of the CIS film are difficult to control.

Differences exist between films formed using different Se sources. Using H_2Se yields the fastest Se incorporation into the absorber. Use of H_2Se also provides the best compositional uniformity and the largest grain sizes. However, H_2Se is highly toxic and is classified as hazardous to the environment.

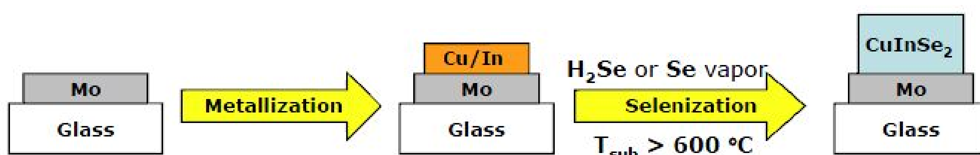

Fig. 7 Schematic for metallic layers followed by selenization process

AVANCIS GmbH and Co. KG formed an elemental precursor film by DC-magnetron sputtering of I-III-VI_2 compound and the thermal evaporation of Se followed by RTA in a sulfur containing ambient. Jheng *et al.* prepared I-III-VI_2 thin films by co-sputtering with Cu-Ga alloy and In-Se alloy targets before a two-step annealing process without an additional Se source under vacuum.

In this thesis, a non-selenization process is proposed to prepare CIS thin films. Co-sputtering method with In and $CuSe_2$ targets would produce a smoother surface and better crystallinity in the absorber, when compared to a stacked multilayer (Cu/In/Ga/Cu/In/Ga⋯) structure or a simple bilayer (CuSe alloy/InSe alloy) or trilayer (Cu/In/Se) as a precursor (See Fig. 8). These attributes result in higher efficiency devices.

This co-sputtering process with $CuSe_2$ target followed by RTA process has many advantages including simplicity without an additional H_2Se or Se vapor in RTA process, large-area manufacturing for mass production, and excellent electrical and optical properties. Another merit of this novel method is the ease of adjusting chemical composition ratio in I-III-VI_2 thin films.

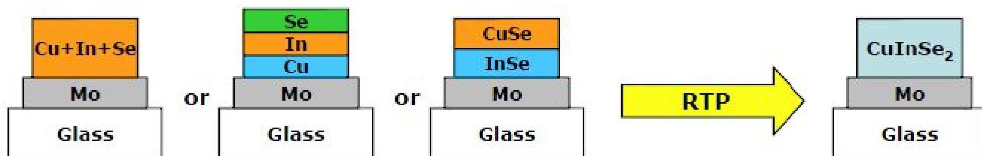

Fig. 8 Proposed method for preparing CIS thin films without an additional H_2Se or Se vapor in RTA process

D. Characterization of Thin Films

A number of processes can occur, including reflection, scattering, absorbance, fluorescence/phosphorescence (absorption and re-emission), and photochemical reaction (absorbance and bond breaking) when radiation interacts with matter. In general, optical transmission are calculated by measuring the absorbance from UV-visible spectroscopy.

When light passes through or is reflected from a sample, the amount of light absorbed is the difference between the incident radiation (I_o) and the transmitted radiation (I). The amount of light absorbed is expressed as either transmittance or absorbance. Optical transmittance usually is given in terms of a fraction of 1 or as a percentage and is defined using the Beer-Bouguer-Lambert Law as follows:

$$T = I / I_0 \quad or \quad \%T = (I / I_0) \times 100 \qquad (2\text{-}1)$$

Absorbance of the thin films was examined at a certain wavelength of light using the equation,

$$A = - \log T = \log I_0 / I \qquad (2\text{-}2)$$

, where A is the absorbance, T is the transmittance, I_0 is the intensity of incident radiation, and I is the intensity of transmitted radiation. Absorption coefficient (α) which was calculated using the Beer-Lambert law in the high-absorption region [24,25]:

$$\alpha (\upsilon) = (2.303 / d) A \qquad (2\text{-}3)$$

, where d and A are the film thickness and film absorbance, respectively. This can be explained using the reciprocal of the penetration depth ($\alpha = 1 / \Gamma$). The penetration depth (Γ) is a measure of how far an incident

photon with a given wavelength penetrates (not absorbed) below the surface of a thin film to a depth at which the irradiance decreases to 37% (*i.e.*, *1 / e*) of its incident level [26,27].

For direct band gap materials such as CIS, the band gap (E_g) can be obtained by an extrapolation in the linear region of each curve to the energy axis from the Tauc plot of $(\alpha h\upsilon)^2$ vs. the photon energy ($h\upsilon$). The band gap energy is found where the fitted line intercepts the energy-axis. The band gap (E_g) of CIS thin films were also calculated using the equation

$$E_g = hc / \lambda \tag{2-4}$$

, where h is Planck's constant (4.135667×10^{-15} eVs), c is the velocity of light (3×10^{8} m/s) and λ is the wavelength (nm) of the absorption onset (1 / e = 37%).

By measuring the Hall effect in a semiconductor one may obtain the mobility and the free carrier density of the material in addition to the resistivity. Also whether the sample is of n-type or p-type conductivity can be determined. The origin of the Hall effect is the force that acts on electrons that move perpendicular to a magnetic field. This force sets up the so called Hall voltage (V_H) in the direction perpendicular to the magnetic field and the current. This voltage is included in the definition of the Hall coefficient (R_H).

$$R_H = tV_H / BI \tag{2-5}$$

In Equation (2-5), the assumption is that the magnetic field is perpendicular to the film surface. The sign of R_H will be different depending on if the conduction in the films is due to holes or electrons. Therefore, the carrier density is given by one or the other of the following expressions.

$$p = 1 / qR_H \quad or \quad n = -1 / qR_H \qquad (2\text{-}6)$$

If both carrier types contribute to the conduction the situation is more complicated. For simplicity energy-independent carrier scattering mechanisms is assumed when deriving Equation (2-6). This simplification is usually done when evaluating thin films. The majority carrier mobility is then calculated from Equation (2-7).

$$\mu = |R_H| / \rho \qquad (2\text{-}7)$$

Van der Pauw method can be used to evaluate the carrier density and mobility of the thin films. In this technique the films should be uniformly thick and not include any isolated holes. The contacts should be ohmic, sufficiently small and positioned at the circumference of the sample. In the Van der Pauw-method a number of resistance measurements are made. For each measurement the current is driven between two contacts while the voltage simultaneously is measured at the two other contacts. For resistivity determination, measurements are made between neighbouring contacts without magnetic field. Carrier density and mobility are calculated from measurements between opposite contacts with magnetic field applied.

III. Experimental Details

A. Preparation of Thin Films

Corning glass (20×20 mm^2) was used as a substrate for deposition of 500-nm thin films by RF magnetron co-sputtering (IDT Engineering Co.). Before the deposition of the thin films, the substrates were cleaned using ultrasonication and dried in nitrogen.

Commercial $CuSe_2$ (TASCO, 99.99% purity, 2 inches-diameter) and In (MTI Co. Inc., 99.99% purity, 2 inches-diameter) targets were used with the following fixed process parameters: pre-sputtering for 3 minutes, Ar gas flux of 50 sccm, base pressure of 1.0×10^{-6} Torr, 5.0 cm distance from the substrate to targets and vacuum pressure of 7.5×10^{-3} Torr during the sputtering process at room temperature.

Fig.9 Photograph of co-sputtering equipment (IDT Engineering Co.)

RF sputtering powers for In target were changed from 10 to 30 W with an interval of 5 W, when that for $CuSe_2$ target was fixed at 65 W to control the chemical composition in the thin films. With considering different deposition rates of each target, the co-sputtering times were also changed by 49, 34, 25, 23 and 21 minutes, respectively, to maintain the total thickness of the co-sputtered $CuSe_2$ and In thin films at approximately 500 nm, as measured by X-ray reflectometry (XRR). The process parameters were summarized in Table 1.

Table 1. Process conditions in co-sputtering for CIS thin films

Target	Co-sputtering Time [min]	49	34	25	23	21
$CuSe_2$	Power [W]	65	65	65	65	65
	Deposition Rate [nm/min]	6.92	6.92	6.92	6.92	6.92
	Thickness [nm]	339.1	235.3	173.0	159.2	145.3
In	Power [W]	10	15	20	25	30
	Deposition Rate [nm/min]	3.42	7.93	12.45	14.11	15.78
	Thickness [nm]	167.6	269.6	336.2	324.5	299.8
Total Thickness [nm]		506.7	504.9	484.3	483.7	476.7
Cu/In Ratio		1.48	3.44	5.40	6.12	6.84

B. Rapid Thermal Annealing for Thin Films

Annealing of the thin films was performed to form the CIS chalcopyrite (112), (220) / (204), and (312) / (116) phases by RTA without a selenium / sulfur containing gas. The RTA (Modular Process Technology Co., RTP-600S) treatment of the 500-nm-thick thin films was performed to improve the temperature uniformity over the conventional furnace for 10 seconds in N_2 gas ambient at a fixed temperature of 400℃ [28,29]. A non-selenization / non-sulfurization process was performed during the RTA treatment for preparing CIS thin films without additional Se- / S-containing gas.

Fig.10 Photograph of rapid thermal annealing (Modular Process Technology Co., RTP-600S)

C. Characterization of Thin Films

The crystalline structure of the thin films was analyzed by X-ray diffraction (XRD, Philips, X' pert-PRO-MRD, Cu Kα = 0.15405 nm, 40 kV, 30 mA) over the scan range, 10 - 90° 2θ.

Energy-dispersive X-ray (EDX, Oxford Instruments, INCA) installed in the field emission scanning electron microscope (FESEM, JEOL, JSM-7500F) was used to characterize the chemical composition ratio of each element in the as-deposited and RTA-treated thin films with a change of sputtering powers for In target from 10 to 30 W at the fixed sputtering power for $CuSe_2$ target of 65 W.

The optical properties of the as-deposited and RTA-treated thin films were measured using an ultraviolet-visible spectrophotometer (BaySpec Inc., UNIR-230) in the range, 400 - 1500 nm. The electrical properties of the thin films, including the carrier concentration, resistivity and mobility were characterized using a Hall Effect measurement system (Accent Optical Technologies, HL5500PC) at room temperature.

Fig. 11. Photographs of HR UV-VIS-NIR spectrophotometer and Hall effect measurement system

Ⅳ. Results and Discussion

Figure 12 shows XRD patterns of the as-deposited $CuSe_2$/In precursors with different sputtering powers for In target in co-sputtering process; (a) 10, (b) 15, (c) 20, (d) 25 and (e) 30 W at the fixed power of 65 W for $CuSe_2$ target with a change of co-sputtering times for 49, 34, 25, 23 and 21 minute, respectively. The XRD patterns were obtained by scanning 2θ in the range of 10 - 90° . The as-deposited $CuSe_2$/In precursors thin films by co-sputtering method showed a broad and weak peak at approximately 27° 2θ corresponding to the position of the (112) peak of CIS, confirming the almost amorphous nature. Any significant peak related to the crystalline phases of Cu, Se and In did not appear, which means that the microstructure remained amorphous regardless of the sputtering power for In target.

The XRD patterns became sharper / stronger after RTA treatment for 10 seconds, indicating enhanced crystalline quality in CIS thin films. The RTA-treated thin films showed the major diffraction peaks corresponding to CIS chalcopyrite phases with preferred orientations in Fig. 13: (112), (220)/(204) and (312)/(116) at 26.67° , 44.29° and 52.42° 2θ [4,5,9,12,30]. All the peaks corresponded the above CIS chalcopyrite phases in the RTA-treated specimens only with sputtering powers for In target of (c) 20 and (d) 25 W. The XRD patterns of the RTA-treated specimens with these powers for In indicated that the crystallinity and the grain growth of the CIS thin films had occurred along the above CIS crystallographic planes with (112), (220)/(204) and (312)/(116) orientations.

This confirms that this method can achieve good crystallization quality and grain growth. Sufficient electrical properties including the open circuit voltage (V_{oc}) and short circuit current density (J_{sc}) can be obtained by reducing the carrier recombination and structural

defect-originated leakage current in the thin films by the densely packed (112), (220)/(224), and (312)/(116)-oriented grains [4].

The RTA-treated specimens with relatively lower sputtering powers for In target of (a) 10 and (b) 15 W showed the strong XRD peak at 31.09° *2θ* corresponding to the position of the (222) peak of In_2O_3 [31]. Some of the small peaks were also observed in the same specimens at 27.55°, 41.89° and 45.91° *2θ* corresponding to the position of the (103), (213)/(105) and (301) peaks [32]. The presence of small peaks in XRD patterns indicates that small grains have been formed and the grain growth had been insufficient along the various orientations not along the above preferred orientations in these powers for In target.

The (220)/(204) and (312)/(116) diffraction peaks were not detected and (112) peak became weaker in the RTA-treated specimens with a relatively higher sputtering power for In target of (e) 30 W. This result coincided with that of a prior literature in which the XRD diffraction peaks gradually decreased when the In/Cu ratio in the film increased over 0.4 [33].

Moreover, both peaks corresponding to the (220)/(204) and (312)/(116) orientations shifted to lower *2θ* values with increasing sputtering powers for In target (Fig. 13), which is consistent with the well-known shift in the diffraction peaks to a lower angle with increasing In content due to the increase in the '*a*' and '*c*' lattice constants. Hence, the *d* spacing decreases with the further addition of larger In atoms into $CuSe_2$ lattice [32-36]. Therefore, XRD suggests that polycrystalline CIS was rebuilt on the substrate, and the crystallinity could be modified by changing the sputtering powers for In target in co-sputtering process.

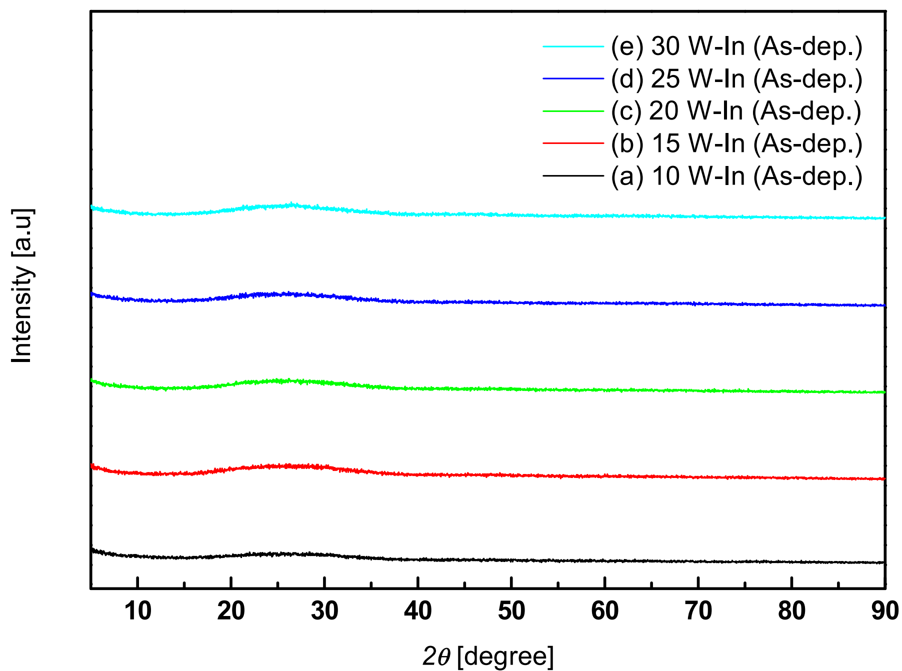

Fig. 12 XRD patterns of the as-deposited CIS thin films at the various sputtering powers of 10, 15, 20, 25, and 30 W for In target at the fixed power of 65 W for $CuSe_2$ target with a change of co-sputtering times for 49, 34, 25, 23 and 21 minute, respectively

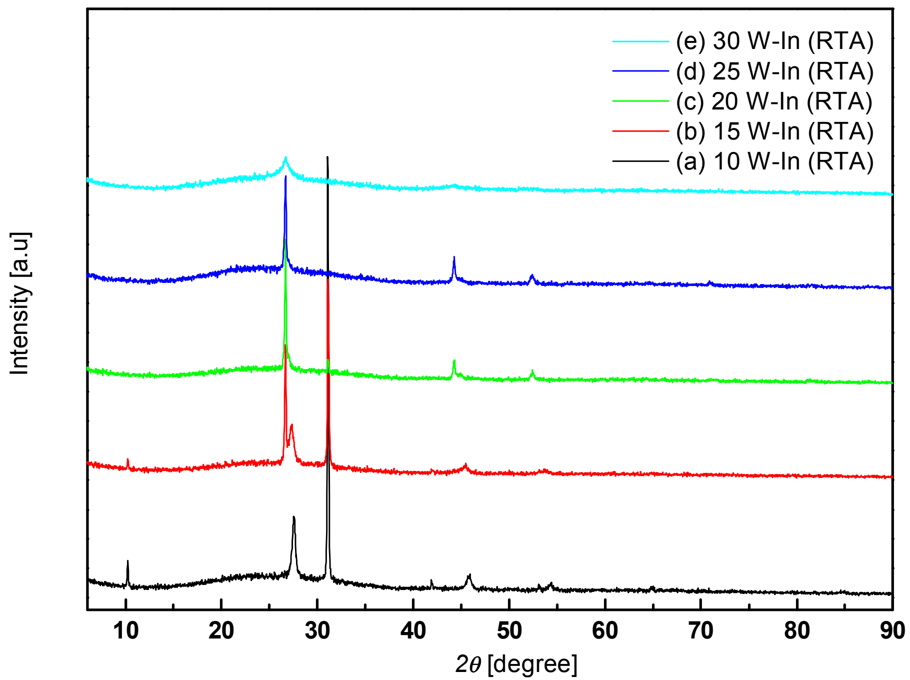

Fig. 13 XRD patterns of the RTA-treated (400℃ for 10 seconds in N_2 gas ambient) CIS thin films at the various sputtering powers of 10, 15, 20, 25, and 30 W for In target at the fixed power of 65 W for $CuSe_2$ target with a change of co-sputtering times for 49, 34, 25, 23 and 21 minute, respectively

The lattice constants, *a* and *c*, of the tetragonal structure were calculated using the equation,

$$1 / d_2 = (h_2 + k_2) / a_2 + l_2 / c_2 \quad (4\text{-}1)$$

, combined with the Bragg's law,

$$d = \lambda / 2\sin\theta \quad (4\text{-}2)$$

, where *d* is the spacing between the planes in the atomic lattice (inter-planar spacing), *hkl* are Miller indices, λ is the wavelength of Cu Kα radiation (λ = 0.15406 nm) and θ is the angle between the incident ray and the scattering planes [37]. For a particular incident X-ray wavelength, λ, and the angle, θ from XRD, the *d* spacing can be determined from Bragg's law. The lattice constants, *a* and *c*, can also be calculated using the (112), (220)/(204) and (312)/(116) peaks.

The inter-planar spacing of the (112) peak ($d_{(112)}$) in the RTA-treated CIS thin films at the various sputtering powers for In target was calculated using (4-2) and is shown in Fig. 14. The $d_{(112)}$ increased slightly with sputtering power for In target up to (b) 20 W, indicating better crystallinity due to the decrease in the number of crystallographic rearrangement-induced structural defects and internal stresses, as reported by Bouraiou *et al.* [38]. Then, the $d_{(112)}$ decreased rapidly with an increase in sputtering powers for In target, which was attributed to the further addition of larger In atoms into $CuSe_2$ lattice, as mentioned above [33].

The tetragonal distortion parameter in the RTA-treated CIS thin films at the various sputtering powers for In target,

$$\eta = c / 2a \quad (4\text{-}3)$$

, was in the range of 1.336 - 1.433, as shown in Fig. 14 which is larger than the value of 1.003 - 1.008 reported for most chalcopyrite tetragonal crystals [39,40]. The distortion parameter in CIS thin films was strongly affected by the chemical composition of the CIS thin films [41].

Fig. 15 shows the chemical compositions of the as-deposited and RTA-treated CIS thin films with various sputtering powers for In target. The specimens were taken from a depth of 30 nm on each surface to obtain the atomic percentages of CIS thin films by EDX. The contents of Cu, In and Se in the as-deposited specimens were shown in the dotted lines. The relative atomic percentage of In was confirmed to show an increase-tendency from 5.12 to 28.42% with sputtering powers for In target from 10 to 30 W, where those of Cu and Se decreased from 37.02 and 57.87 to 24.85 and 46.73%, respectively.

The atomic percentages of Se after RTA-treatment (solid lines) decreased in the all conditions of sputtering power for In target compared to those in the as-deposited specimens due to its well-known volatility in high temperature [28,29]. In the RTA-treated specimens, the relative atomic percentage of Cu decreased up to 20 W of the sputtering power for In target and then showed an increase-tendency, while that of In showed an exactly inverse tendency to Cu.

The deviation from the chemical composition was used with the two parameters,

$$\Delta m = [Cu]/[In] - 1 \tag{4-4}$$

and

$$\Delta s = 2[Se]/([Cu]+3[In]) - 1 \tag{4-5}$$

[41], which means that the material is stoichiometric when both parameters show no deviation. The as-deposited CIS thin films had Δm = 6.23, 2.40, 1.17, 0.95, and − 0.13, while Δs = 1.21, 0.60, 0.31, 0.31 and − 0.15 with increasing sputtering powers for In target. The Cu-rich ($\Delta m > 0$) and Se-excess ($\Delta s > 0$) composition was obtained in all the as-deposited

specimens except a condition with the relatively higher sputtering power for In target of (e) 30 W. The Cu-poor (Δm < 0) and Se-poor (Δs < 0) composition was shown in this condition.

Fig. 16 shows the deviation parameters of Δm and Δs in the RTA-treated specimens with various sputtering powers for In target. The RTA-treated CIS thin films had Δm = 4.49, 2.07, 0.00, 1.53, and 1.13, while Δs = 0.42, 0.23, - 0.21, - 0.14 and - 0.08 with increasing sputtering powers for In target. The Cu-rich (Δm > 0) composition was obtained in all the RTA-treated specimens except a condition with the sputtering power for In target of (c) 20 W. The Se-excess (Δs > 0) composition was obtained in the RTA-treated specimens with relatively lower sputtering powers for In target of (a) 10 and (b) 15 W, while the Se-poor (Δs < 0) composition was shown in the conditions from (c) 20 to (e) 30 W.

When both deviations of Δm and Δs become close to '0' in the CIS thin film, the CIS thin film generally indicates an approach to a near-stoichiometric composition. In a condition of (c) 20 W, the contents of Cu and In approached the near-stoichiometry, but content of Se was somewhat insufficient to the near-stoichiometry. However, this condition is the nearest stoichiometry in the results of this thesis. The RTA-treated CIS thin films showed a Cu-rich and Se-excess composition in (a) 10 and (b) 15 W as well as a Cu-rich and Se-poor composition in (a) 25 and (b) 30 W.

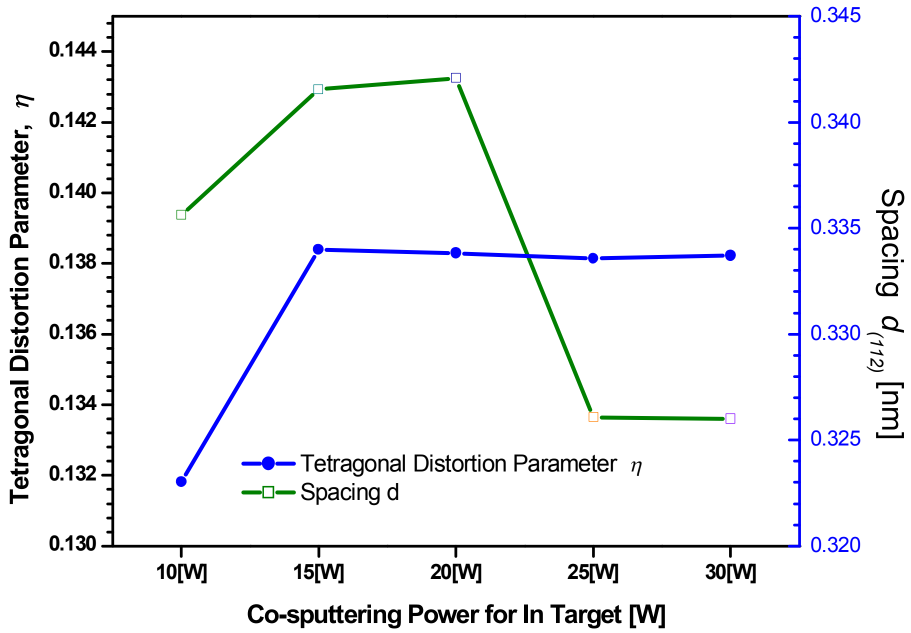

Fig. 14 Distortion parameter η and inter-planar spacing $d_{(112)}$ of the RTA-treated (400℃ for 10 seconds in N_2 gas ambient) CIS thin films at the various sputtering powers of 10, 15, 20, 25, and 30 W for In target at the fixed power of 65 W for $CuSe_2$ target with a change of co-sputtering times for 49, 34, 25, 23 and 21 minute, respectively

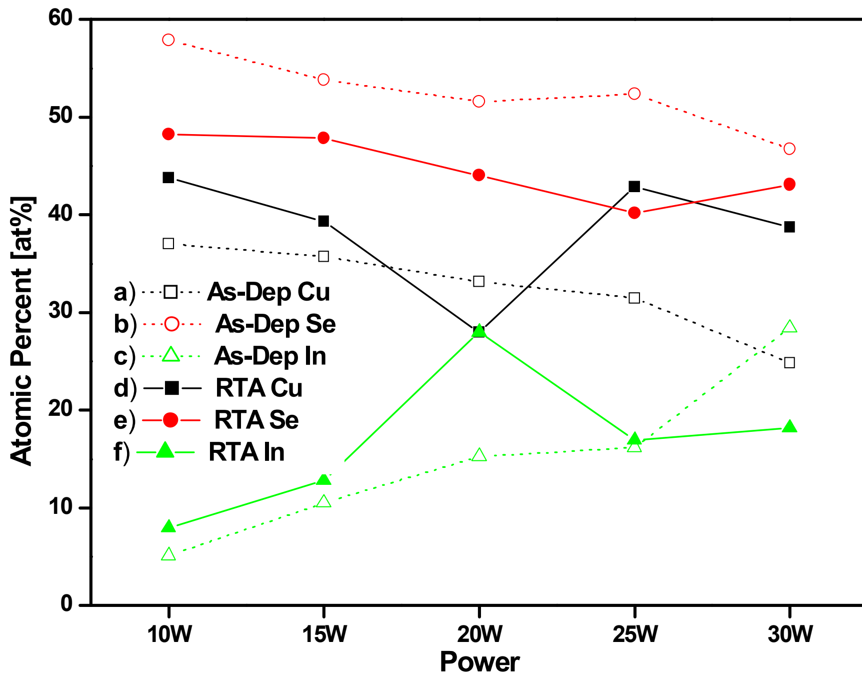

Fig. 15 Atomic percent of the as-deposited and RTA-treated (400℃ for 10 seconds in N_2 gas ambient) CIS thin films at the various sputtering powers of 10, 15, 20, 25, and 30 W for In target at the fixed power of 65 W for $CuSe_2$ target with a change of co-sputtering times for 49, 34, 25, 23 and 21 minute, respectively

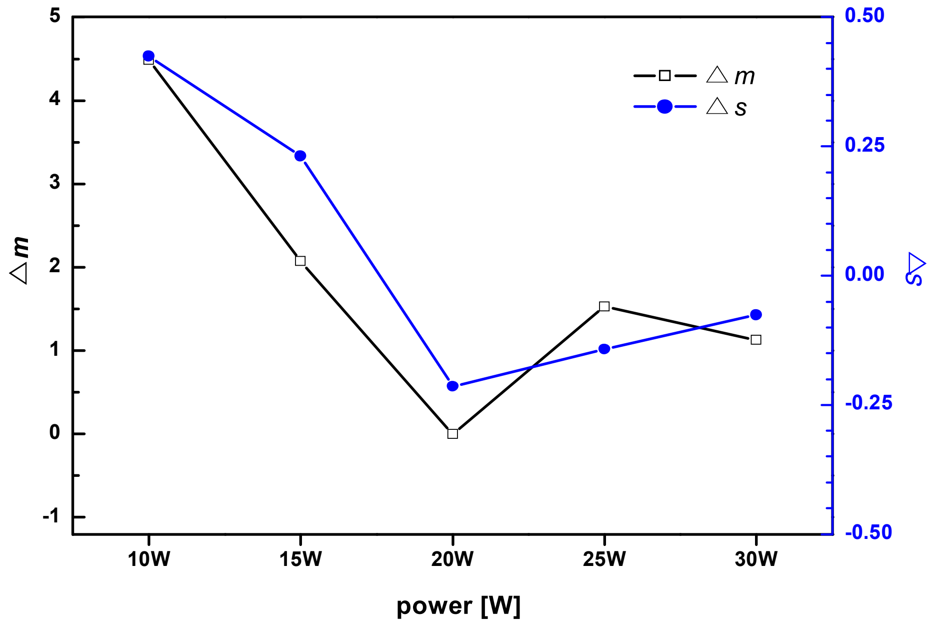

Fig. 16 Deviation parameters of Δm = [Cu]/[In] -1 and Δs = 2[Se]/([Cu]+3[In]) -1 from the chemical compositions of the RTA-treated (400℃ for 10 seconds in N_2 gas ambient) CIS thin films at the various sputtering powers of 10, 15, 20, 25, and 30 W for In target at the fixed power of 65 W for $CuSe_2$ target with a change of co-sputtering times for 49, 34, 25, 23 and 21 minute, respectively

Fig. 17 shows the optical transmittance in the visible to near-infrared (NIR) spectral region of the as-deposited CIS thin films. All spectra were ≤ 32% in the visible spectral region (400 - 800 nm), and the mean optical transmittance was also ≤ 12% over the same wavelength range. The mean optical transmittance of the as-deposited CIS thin films were 0.30% and 2.14% with relatively lower sputtering powers for In target of (a) 10 and (b) 15 W, respectively, which were somewhat lower than those with relatively higher sputtering powers for In target of (d) 25 and (e) 30 W (11.89% and 12.16%).

Throughout the visible spectral region (400 - 800 nm), the as-deposited CIS thin films revealed considerable absorption because all the spectra converged to the '0' value regardless of the sputtering powers for In target (*i.e.* content of In). But, the contrary to the Burstein-Moss (B-M) shift was also observed as an increase in the sputtering power for In target. B-M shift is the absorption edge shifted to a larger wavelength, highlighting the advantages of CIS thin films as the absorber layer in thin film photovoltaic devices due to the decrease in the range of spectral transmission to the minimum of the solar emission spectrum [42-44]. The observation of this contrary to the B-M shift means that disadvantage of the CIS thin film as an absorber layer was caused by the sputtering power for In target (*i.e.* content of In).

When the wavelength range was widened from visible spectral region to the NIR spectral region (400 - 1500 nm), the mean optical transmittance of the as-deposited CIS thin films with relatively lower sputtering powers for In target of (a) 10 and (b) 15 W increased gradually to 17.57% and 29.84%, respectively, whereas those with relatively higher sputtering powers for In target of (c) 20 and (d) 25 W increased rapidly to 32.96% and 34.10% over the same spectral range.

The experimentally-measured optical transmittance of the RTA-treated CIS thin films was also represented in the visible to NIR spectral region, as shown in Fig. 18. All spectra were ≤ 15% in the visible spectral

region (400 - 800 nm), and the mean optical transmittance was also ≤ 9% over the same wavelength range. The optical transmittance increased somewhat in the all conditions after RTA-treatment. The mean optical transmittance of the RTA-treated CIS thin films was 6.29% in the sputtering power for In target of (a) 10 W, which were somewhat higher than those with relatively higher sputtering powers for In target of (b) 15, (c) 20 and (d) 25 W corresponding to 5.49%, 5.82% and 5.69%.

The RTA-treated CIS thin films also revealed considerable absorption throughout the visible spectral region (400 - 800 nm) regardless of In-content. The contrary to the B-M shift was similarly observed as increasing the sputtering power for In target, however, the shifted absorption edges were located in the similar wavelength in the visible spectral region except a condition of (e) 30 W.

The mean optical transmittance of the RTA-treated CIS thin films with relatively lower sputtering powers for In target of (a) 10, (b) 15 and (c) 20 W increased gradually to 9.72%m, 9.62% and 13.01%, respectively, when the wavelength range was widened from visible spectral region to the NIR spectral region (400 - 1500 nm), whereas that with the sputtering powers for In target of (d) 25 and (e) 30 W increased rapidly to 19.21% and 31.05% over the same spectral range.

Compared to the as-deposited CIS thin films, this indicates that the RTA-treated CIS thin films showed the better optical transmittance property as an absorber layer especially in the widened spectral region to NIR.

The equation (2-4), $E_g = hc / \lambda$, was used to calculate the optical band gap energies (E_g) of the CIS thin films with the same thickness (approximately 500 nm), where h is Planck's constant (4.135667×10^{-15} eVs), c is the velocity of light (3×10^8 m/s) and λ is the wavelength (nm) of the absorption onset ($1 / e$ = 37%). The optical band gap energy of the RTA-treated CIS thin films were in the range of 0.98 - 1.49 eV with a change of the sputtering power for In target (*i.e.* content of In), as

shown in Fig. 19.

Note that the optical band gap energy of the RTA-treated CIS thin film showed the inverse tendency to the deviation parameter, Δm, in Fig. 16. The optical band gap energy of the RTA-treated CIS thin film was attributed to the composition of In (Fig. 16) and spacing d (crystallinity) (Fig. 14). This result agrees well with previous studies on the optical band gap energy, which attributed this to both crystallinity and intrinsic defects that cause a shift in the absorption edge followed by the RTA treatment [45]. Ramana *et al.* reported that an increase in grain size leads to a decrease in the optical band gap energy due to the fewer free carrier concentrations and lower potential barriers originating from large particles with fewer grain boundaries and imperfections [46].

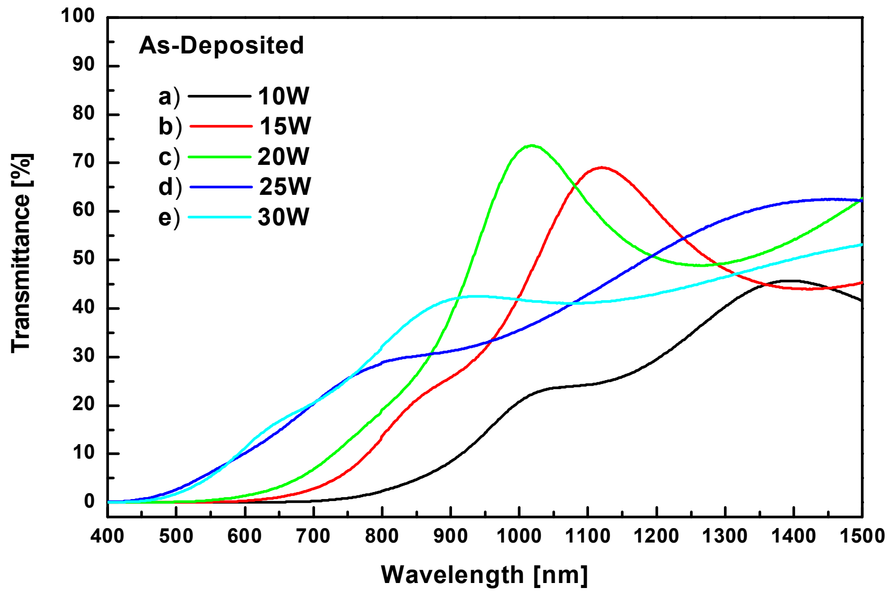

Fig. 17 Optical transmittance of the as-deposited CIS thin films at the various sputtering powers of 10, 15, 20, 25, and 30 W for In target at the fixed power of 65 W for $CuSe_2$ target with a change of co-sputtering times for 49, 34, 25, 23 and 21 minute, respectively

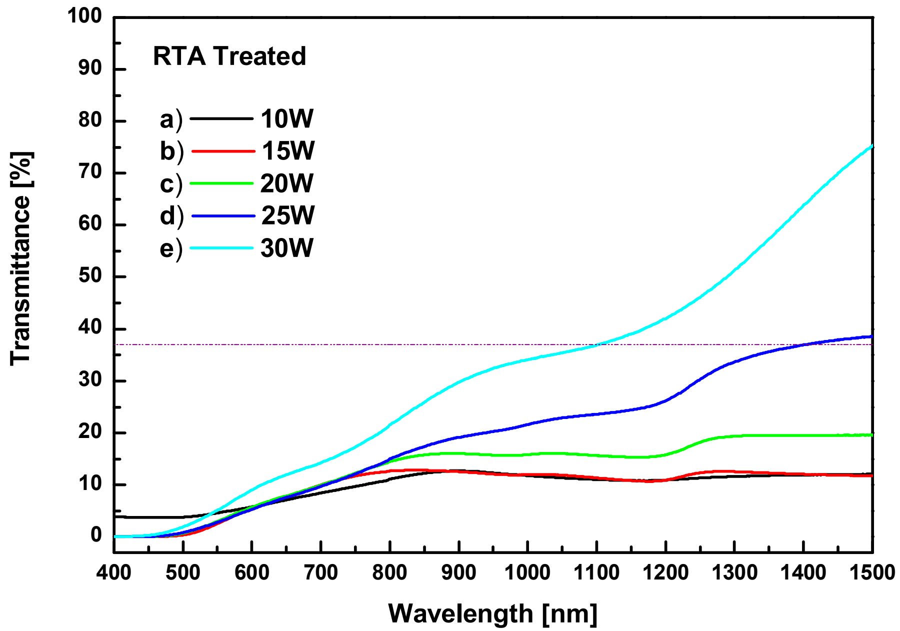

Fig. 18 Optical transmittance of the RTA-treated (400℃ for 10 seconds in N_2 gas ambient) CIS thin films at the various sputtering powers of 10, 15, 20, 25, and 30 W for In target at the fixed power of 65 W for $CuSe_2$ target with a change of co-sputtering times for 49, 34, 25, 23 and 21 minute, respectively

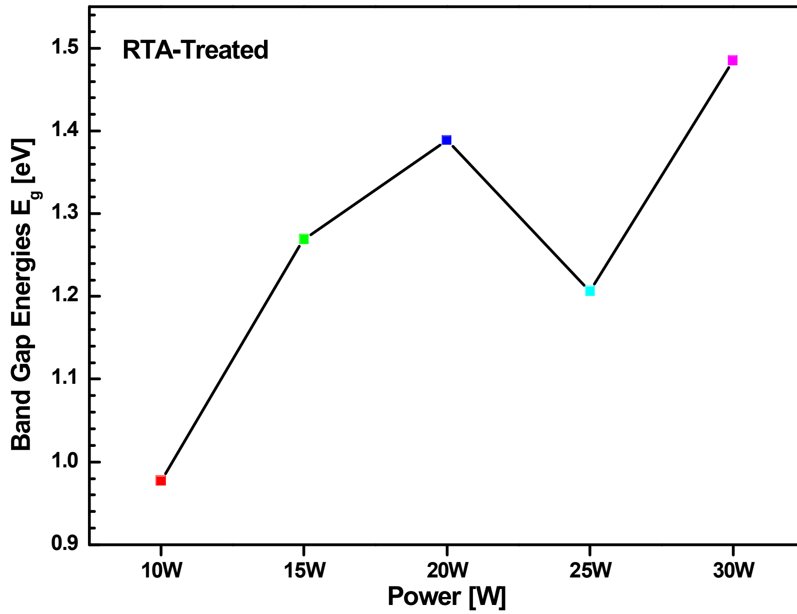

Fig. 19 The calculated optical band gap energies (E_g) of the RTA-treated (400℃ for 10 seconds in N_2 gas ambient) CIS thin films at the various sputtering powers of 10, 15, 20, 25, and 30 W for In target at the fixed power of 65 W for $CuSe_2$ target with a change of co-sputtering times for 49, 34, 25, 23 and 21 minute, respectively

Figures 20 and 21 present the absorption coefficient (α) of the as-deposited and RTA-treated thin films, which was calculated using the equation (2-3) of Beer-Lambert's law in the high absorption region [47,48]: $\alpha(\upsilon) = (2.303/d)A$, where $\alpha(\upsilon)$, d and A are the absorption coefficient, film thickness and film absorbance, respectively. The absorption coefficient is a measure of how far an incident photon of a particular wavelength is absorbed below the surface of the CIS thin film, *i.e.* the ability of a semiconductor to absorb photons [49,50]. This can be expressed as

$$\alpha = (1/d)\ln[(1-R)/T] \qquad (4-6)$$

, where d, R and T is the film thickness, reflectance and optical transmittance, respectively [51]. The absorption coefficient of the CIS thin film was high (approximately 10^4 cm^{-1}) in the visible spectral region, but decreased in the NIR region.

The absorption coefficient of the as-deposited CIS thin films was located over a larger wavelength with a relatively lower sputtering power for In target of (a) 10 W and on the shorter wavelength with an increase in the sputtering power for In target up to (d) 25 or (e) 30 W, as shown in Fig. 20. As shown in the above formula (4-6) and Figs. 17 and 18, the absorption coefficient of CIS thin films with the same thickness was affected directly by the optical transmittance. The lower optical transmittance of the as-deposited CIS thin films with a small amount of In-addition due to impurity-scattering was attributed to the enhanced absorption coefficient in the visible spectral region (400 - 800 nm): The increased defect density by addition of In into $CuSe_2$ lattice is thought to induce more phonon scattering and prevent the incident visible light from transmitting through the as-deposited CIS thin film [52]. This result is similar to a previous report where the optical absorption showed scattering in the visible region as a result of the poor dispersibility of

the dopant [53].

The absorption coefficient of the RTA-treated CIS thin films was also shifted from larger wavelength to shorter wavelength with an increase in the sputtering power for In target except a condition of (a) 10 W, as shown in Fig. 21. Small grains were formed and the insufficient grains grew along the various orientations not along the preferred orientations in the condition of 10 W (See Fig. 13). This phenomenon was attributed to decrease in intrinsic defects (grain boundaries, dislocations, stacking fault, etc.) along with an increase in crystallinity with the sputtering powers for In target of (b) 15 and (c) 20 W, which cause a shift in the absorption edge to the larger wavelength in these powers [45]. Then, the further addition of larger In atoms into $CuSe_2$ lattice lead to decrease in *d* spacing, which induced polycrystalline CIS to rebuilt on the substrate, and the crystallinity could be modified by changing the sputtering powers for In target in co-sputtering process.

The absorbance can be calculated using the formula (2-2), $A = -\log T = \log I_0 / I$, where A is the absorbance, T is the transmittance, I_0 is the intensity of incident radiation and I is the intensity of transmitted radiation at a certain wavelength. The absorbance of the as-deposited CIS thin films was represented in Fig. 22(a), which presents the mean values in the range from 400 to 1500 nm. The mean absorbance of the as-deposited CIS thin film was in the range of 0.66 - 1.78, which means that approximately 54.6 - 96.0% of the incident photons in the range from 400 to 1500 nm could be absorbed by this approximately 500-nm-thick as-deposited CIS thin films. The mean absorbance was enhanced with a RTA treatment, as shown in Fig. 22(b). The maximum mean value of the RTA-treated CIS thin films was 1.24 with the sputtering power for In target of (c) 15 W, which suggests that approximately 91.7% of the incident photons in the visible and near-infrared spectral regions was absorbed by this RTA-treated CIS thin film. Good crystallinity with substantial scattering is believed to help the RTA-treated CIS thin films

improve their optical absorption.

The optical band gap energies of the as-deposited and RTA-treated CIS thin films were estimated by linear extrapolation of each curve back to the energy axis from the Tauc plot of $(\alpha h\upsilon)^2$ vs. the photon energy ($h\upsilon$), as shown in Figs. 23 and 24, respectively, where α is the absorption coefficient, h is Planck's constant (4.135667×10^{-15} eVs), and υ is the frequency of the incident photon. The optical band-gap energy of the as-deposited CIS thin film was in the range 1.60 - 2.50 eV. The optical band gap energy of CIS thin films rather increased with the RTA-treatment, as shown in Fig. 24. This shows that the higher optical band gap energy in the RTA-treated CIS thin film allows less efficient harvesting of incident light at shorter wavelengths. Overall Se-loss in CIS thin films after RTA treatment might have a higher optical band gap energy. Compared to the values (0.98 - 1.49 eV) calculated by using the equation (2-4), the estimated values (1.00 - 2.30 eV) by using linear extrapolation were higher in the RTA-treated CIS thin films, but the tendency showed the similar trends.

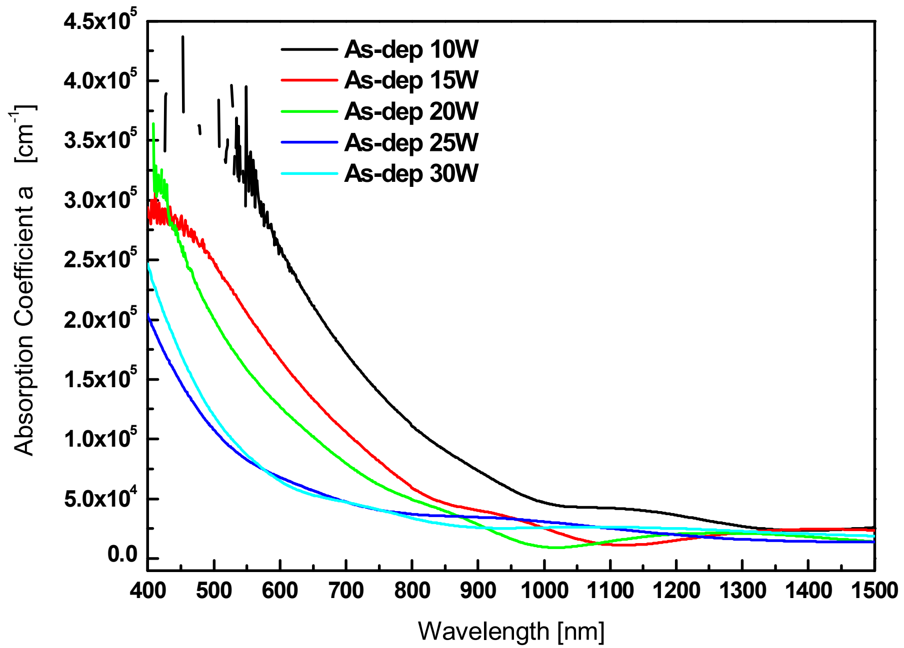

Fig. 20 Absorption coefficient (α) spectra of the as-deposited CIS thin films at the various sputtering powers of 10, 15, 20, 25, and 30 W for In target at the fixed power of 65 W for $CuSe_2$ target with a change of co-sputtering times for 49, 34, 25, 23 and 21 minute, respectively

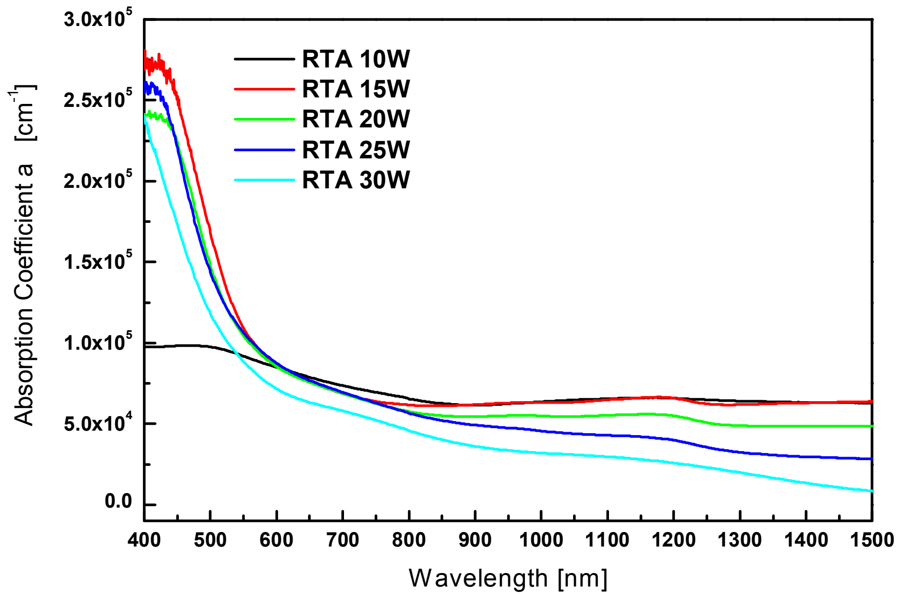

Fig. 21 Absorption coefficient (α) spectra of the RTA-treated (400℃ for 10 seconds in N_2 gas ambient) CIS thin films at the various sputtering powers of 10, 15, 20, 25, and 30 W for In target at the fixed power of 65 W for $CuSe_2$ target with a change of co-sputtering times for 49, 34, 25, 23 and 21 minute, respectively

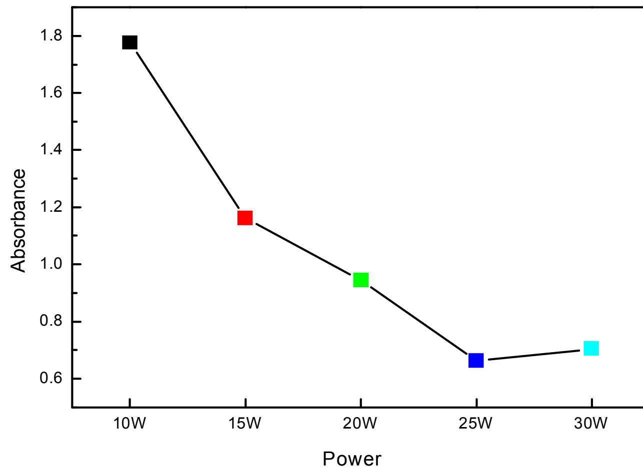

(a)

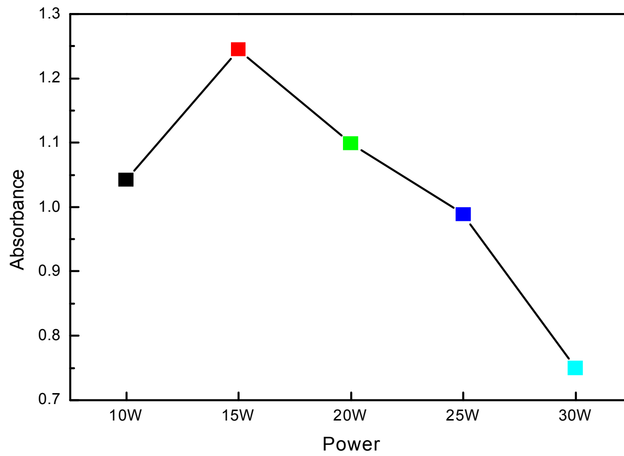

(b)

Fig. 22 Average absorbance in the range of 400 -1500 nm of (a) the as-deposited and (b) RTA-treated (400℃ for 10 seconds in N_2 gas ambient) CIS thin films at the various sputtering powers of 10, 15, 20, 25, and 30 W for In target at the fixed power of 65 W for $CuSe_2$ target with a change of co-sputtering times for 49, 34, 25, 23 and 21 minute, respectively

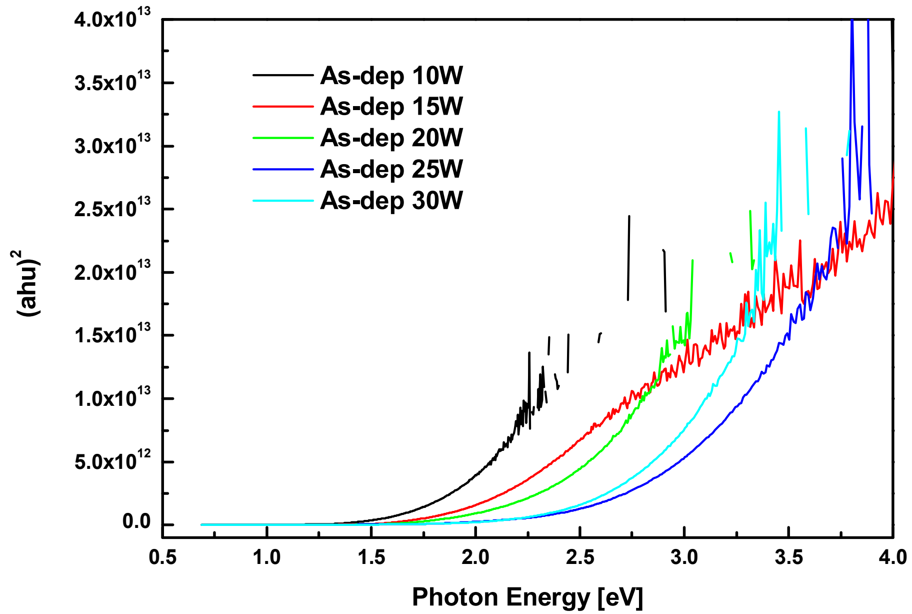

Fig. 23 Tauc plot of $(\alpha h\upsilon)^2$ vs. the photon energy ($h\upsilon$) for the as-deposited CIS thin films at the various sputtering powers of 10, 15, 20, 25, and 30 W for In target at the fixed power of 65 W for $CuSe_2$ target with a change of co-sputtering times for 49, 34, 25, 23 and 21 minute, respectively

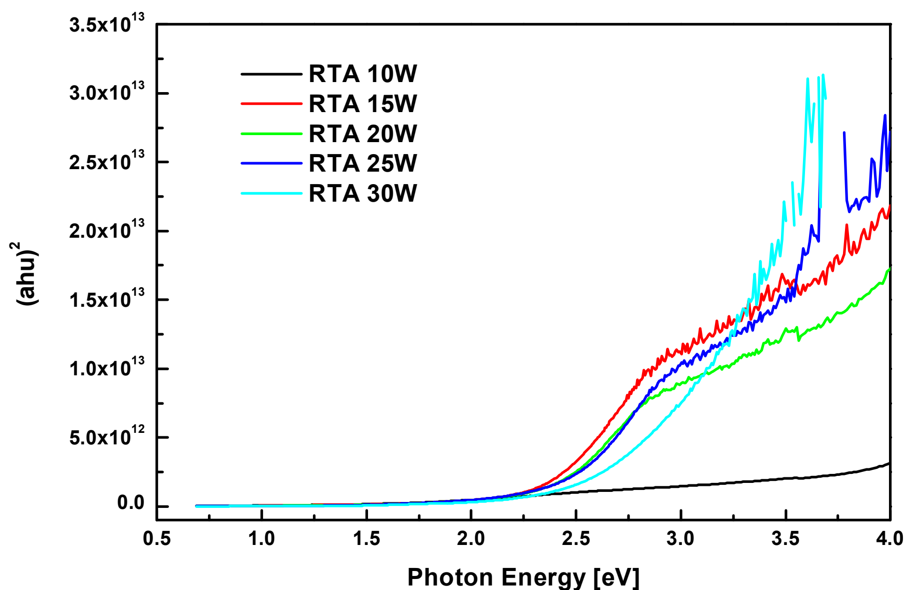

Fig. 24 Tauc plot of $(\alpha h\upsilon)^2$ vs. the photon energy $(h\upsilon)$ for the RTA-treated (400℃ for 10 seconds in N_2 gas ambient) CIS thin films at the various sputtering powers of 10, 15, 20, 25, and 30 W for In target at the fixed power of 65 W for $CuSe_2$ target with a change of co-sputtering times for 49, 34, 25, 23 and 21 minute, respectively

Neumann and Tomlinson reported that the conductivity type was determined by the deviations (Δm and Δs) [54], and Karthikeyan *et al.* have verified and developed the relationship further. They concluded that the CIS thin films in this study with $\Delta m < 0$ and $\Delta s > 0$ always have n-type conductivity [41], and the Hall Effect measurements showed p-type conductivity in all RTA-treated specimens although $\Delta m > 0$ and $\Delta s > 0$ in the conditions of (a) and (b) or $\Delta m > 0$ and $\Delta s < 0$ in the conditions of (d) and (e) (See Fig. 16). P-type conductivity induces better electrical conductivity and higher efficiency in solar cells compared to n-type conductivity [55].

Hall Effect measurements were performed to examine the electrical properties of the as-deposited and RTA-treated CIS thin films, such as the conductivity type, carrier mobility, resistivity, and carrier concentration, with changing sputtering powers for In target, as shown in Figs. 25 and 26.

The carrier concentration of the as-deposited CIS thin films was in the order-range of 10^{15} - 10^{19} cm^{-3} excessive electrons due to n-type conductivity except a condition with a sputtering power for In target of (e) 30 W (10^{20} cm^{-3}-ordered p-type conductivity). The carrier concentration was abruptly changed after RTA treatment, which showed p-type conductivity in the order-range of 10^{17} - 10^{21} cm^{-3} excessive holes in all RTA-treated specimens, as mentioned above. This is similar to the free carrier concentration reported in intrinsic p-type CIS thin films (10^{10} - 10^{21} cm^{-3}) [56,57]. Twelve possible intrinsic defects can exist in CIS thin films; vacancies (V_{Cu}, V_{In}, V_{Se}), interstitials (Cu_i, In_i, Se_i) and anti-site defects (Cu_{In}, In_{Cu}, In_{Se}, Se_{In}, CuS, SeS) [58]. The increased carrier concentration in the CIS thin films was attributed to the reduction in V_{Se} and/or increase in the acceptor centers including V_{Cu}, V_{In}, Cu_{In} and Se_i. Considering the increase in Cu composition in the RTA-treated specimens, the increase in V_{In} is believed to be the main contribution to the increase in carrier concentration. The increase in carrier concentration, acting as

acceptors in p-type CIS thin films, can lead to a decrease in the band gap energy of CIS thin films, which would allow more efficient harvesting of the incident light at longer wavelengths.

The resistivity of the as-deposited and RTA-treated CIS thin films were in the order-range of 10^{-2} – 10^{2} and 10^{-3} – 10^{1} Ω-cm, respectively. The RTA-treated CIS thin films showed the superior values to the reported values (10^{3} - 10^{4} Ω-cm) in the p-type CIS thin films [59]. The high resistivity of the CIS thin films was attributed to the In-rich composition of CIS thin films, which have highly conducting and highly resistive properties with Cu-rich and Cu-poor compositions, respectively [60]. The Cu-rich composition, as shown in Fig. 16, and the carrier concentration caused a decrease in the resistivity of the RTA-treated CIS thin films.

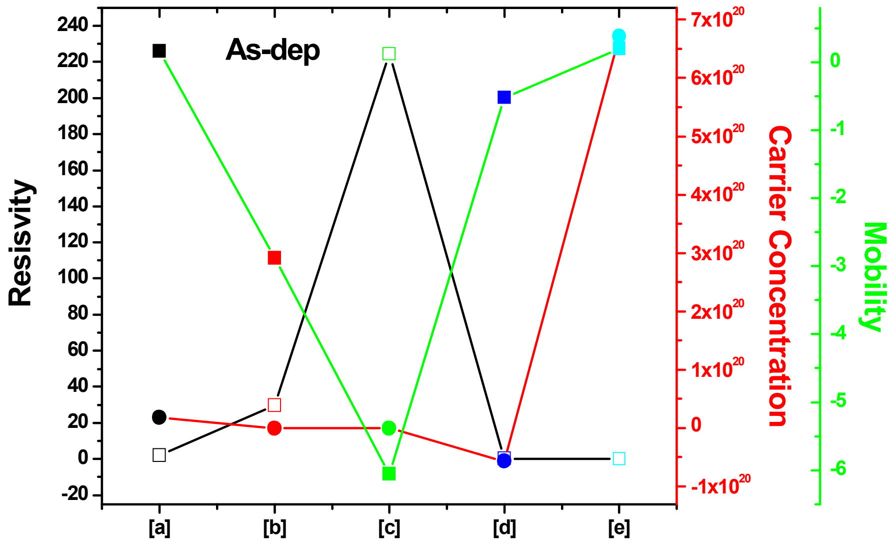

Fig. 25 Hall effect measurements: Resistivity (ρ), carrier concentration (n), and carrier mobility (μ) of the as-deposited CIS thin films at the various sputtering powers of 10, 15, 20, 25, and 30 W for In target at the fixed power of 65 W for $CuSe_2$ target with a change of co-sputtering times for 49, 34, 25, 23 and 21 minute, respectively

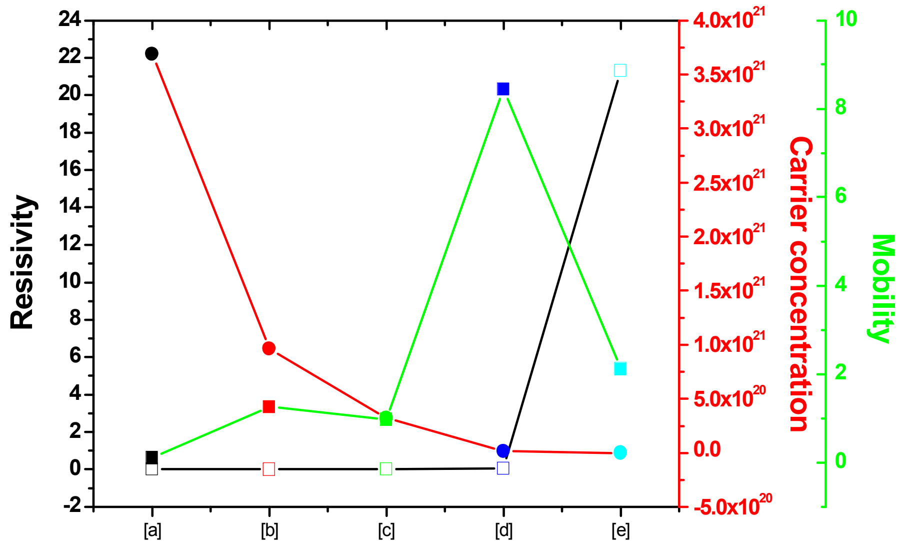

Fig. 26 Hall effect measurements: Resistivity (ρ), carrier concentration (n), and carrier mobility (μ) of the RTA-treated (400℃ for 10 seconds in N_2 gas ambient) CIS thin films at the various sputtering powers of 10, 15, 20, 25, and 30 W for In target at the fixed power of 65 W for $CuSe_2$ target with a change of co-sputtering times for 49, 34, 25, 23 and 21 minute, respectively

Ⅴ. Conclusions

This thesis reported a novel method to fabricate CIS thin films with RTA after co-sputtering by using $CuSe_2$ and In targets without any additional selenization process in annealing process.

Due to the high absorption coefficient and the appropriate band gap energy of 1.04 eV CIS thin films have been used as an absorber layer in the heterostructured thin film solar cell applications, which are considered as the most promising photovoltaic devices in the new and renewable energy industry with the efficiency up to 20%. CIS thin films were generally prepared by using co-evaporation which should require the high-costly equipments for selenization process in selenium-containing gas with hardness to control the accuracy in deposition rate for each element source. However, this method has some critical problems for mass-production including process complexity with costly equipment.

The magnetron co-sputtering method was employed for the preparation for CIS thin films by using In and $CuSe_2$ alloy targets followed by RTA in the N_2 ambient. Generally, the chemical composition ratio of Se was lower than that of the required value for the high-efficiency photovoltaic devices due to its high volatility. The RTA was used for the accurate control of chemical composition ratio of Se for short annealing time at relatively low annealing temperature without aditional Se-containing gas.

Sputtering power for In target was varied to change the stoichiometry of CIS thin films. The structural studies were examined by using an analytical technique of XRD to confirm the CIS chalcopyrite phases and the structural stress in the RTA-treated CIS thin films. An

EDX was employed to examine the chemical states of the as-deposited and RTA-treated CIS thin films. The CIS chalcopyrite (112), (220)/(204), and (312)/(116) phases were clearly formed by the RTA-treated CIS thin films with sputtering powers for In target of 20 and 25 W without a selenium/sulfur containing gas. The atomic percentages of Se after RTA-treatment decreased in the all conditions of sputtering power for In target compared to those in the as-deposited specimens due to its well-known volatility in high temperature. The RTA-treated CIS thin films showed a Cu-rich and Se-excess composition in 10 and 15 W as well as a Cu-rich and Se-poor composition in 25 and 30 W.

The optical properties and electrical characteristics of the RTA-treated CIS thin films were analyzed by using UV-visible spectrophotometer and a Hall Effect measurement system with a change of stoichiometry of the co-sputtered CIS thin films. The optical band gap energy of the RTA-treated CIS thin films were in the range of 0.98 - 1.49 eV with a change of In-content, which showed the inverse tendency to the deviation parameter, Δm. The mean absorbance of the RTA-treated CIS thin films was 1.24 with the sputtering power for In target of 15 W, which suggests that approximately 91.7% of the incident photons in the visible and near-infrared spectral regions was absorbed by this RTA-treated CIS thin film.

The carrier concentration showed p-type conductivity in the order-range of 10^{17} - 10^{21} cm^{-3} excessive holes in all RTA-treated specimens, which is similar to the free carrier concentration reported in intrinsic p-type CIS thin films. The resistivity of the RTA-treated CIS thin films was in the order-range of 10^{-3} - 10^{1} Ω-cm, which showed the superior values to the reported values due to the Cu-rich composition and the high carrier concentration.

REFERENCES

[1] M. Hädrich, C. Kraft, C. Löffler, H. Metzner, U. Reislöhner, W. Witthuhn, Thin Solid Films 517 (2009) 2282-2285.

[2] A. A. Alnajjar, M. F. A. Alias, R. A. Almatuk, A. A. J. Al-Douri, Renew. Energ. 34 (2009) 2160-2163.

[3] N. V. Sochinskii, M. Abellán, J. Rodríguez-Fernández, E. Diéguez, J. Franc, P. Hlidek, P. Praus, V. Babentsov, Superlattice. Microst. 45 (2009) 228-233.

[4] B. T. Jheng, P. T. Liu, M. C. Wu and H. P. D. Shieh, Opt. Lett. 37, 2760 (2012).

[5] Y. C. Lin, J. H. Ke and C. C. Chen, Appl. Mech. Mater. 189, 63 (2012).

[6] O. Schultz, S. W. Glunz and G. P. Willeke, Prog. Photovolt. Res. Appl. 12, 553 (2004).

[7] T. M. Razykov, C. S. Ferekides, D. Morel, E. Stefanakos, H. S. Ullal and H. M. Upadhyaya, Sol. Energy 85, 1580 (2011).

[8] Y. C. Lin, Z. Q. Lin, C. H. Shen, L. Q. Wang, C. T. Ha and C. Peng, J. Mater. Sci. 23, 493 (2012).

[9] C. M. Xu, Y. Sun, L. Zhou, F. Y. Li, L. Zhang, Y. M. Xue, Z. Q. Zhou and Q. He, Chin. Phys. Lett. 23, 2259 (2006).

[10] A. Jager-Waldau, Sol. Energ. Mat. Sol. C. 95, 1509 (2011).

[11] T. Dalibor, S. Jost, H. Vogt, R. Brenning, A. Heiß, S. Visbeck, T. Happ, J. Palm, A. Avellán, T. Niesen and F. Karg, in Proceedings of the 25th European Photovoltaic Solar Energy Conference and Exhibition / 5th World Conference on Photovoltaic Energy Conversion (Valencia, Spain, September 6-10, 2010), p.2854

[12] N. H. Kim, S. Oh and W. S. Lee, J. Korean Phys. Soc. 61, 1177 (2012).

[13] J. Y. C. Liew et al., Cent. Eur. J. Phys. 7, 379 (2009).

[14] Gosavi and Ramphal Sharma, J. Alloy. Compd., Vol. 448, No. 1-2, 2008, pp. 344-348.

[15] G. P. Bernardini and A. Catani, Miner. Depos., Vol. 3, 1968, pp. 375-380.

[16] J. A. N. Malik et al., J. Mater. Res. 24, 1375 (2009)

[17] http://micro.magnet.fsu.edu/primer/java/solarcell

[18] http://en.wikipedia.org/wiki/File:Isolator-metal.svg

[19] http://en.wikipedia.org/wiki/File:Pn-junction-equilibrium.png

[20] H. K. Singh, "CIGS THIN FILM PHOTOVOLTAIC", http://www.ncpre.iitb.ac.in/page.php?pageid=49&pgtitle=CIGS-Thin-Film-Photovoltaic

[21] http://en.wikipedia.org/wiki/File:Chalcopyrite-unit-cell-3D-balls.png

[22] http://www.mawi.tu-darmstadt.de/of/of/forschung_2/of_oxidelektronik/tcos/tcos.en.jsp

[23] http://www.che.ufl.edu/anderson/Photovoltaics.htm

[24] D. Souri and K. Shomalian, J. Non-Cryst. Solids 355, 1597 (2009).

[25] J. M. González-Leal, A. Ledesma, A. M. Bernal-Oliva, R. Prieto-Alcón, E. Márquez, J. A. Angel and J. Cárabe, Mater. Lett. 39, 232 (1999).

[26] N. H. Kim, C. I. Park, J. Park, J. Korean Phys. Soc. 62, 502 (2013).

[27] J. M. P. Coelho, M. A. Abreu and F. C. Rodrigues, Polym. Test. 23, 307 (2004).

[28] K. Bouabid, A. Ihlal, A. Manar, A. Outzourhit, E. L. Ameziane, Thin Solid Films, Vol. 488, 2005, pp. 62-67.

[29] E. Ahmed, A. Zegadi, A. E. Hill, R. D. Pilkington, R. D. Tomlinson, A. A. Dost, W. Ahmed, S. Leppävuori, J. Levoska, O. Kusmartseva, Journal of Materials Science: Materials in Electronics, Vol. 7, No. 3, 1996, pp. 213-219.

[30] A. M. Hermann, C. Gonzalez, P. A. Ramakrishnan, D. Balzar, N. Popa, P. Rice, C. H. Marshall, J. N. Hilfiker, T. Tiwald, P. J. Sebastian, M. E. Calixto and R. N. Bhattachary, Sol. Energ. Mat. Sol. C., Vol. 70, Iss. 3, 2001, pp. 345-361.

[31] G. Chen, W. Liu, G. Jiang, J. Li and C. Zhu, Journal of Alloys and Compounds, Vol. 531, 2012, pp. 91- 95.

[32] M. Venkatachalam, M. D. Kannan, S. Jayakumar, R. Balasundaraprabhu and N. Muthukumarasamy, Thin Solid Films, Vol. 516, 2008, pp. 6848-6852.

[33] L. P. Deshmukh, R. V. Suryawanshi, E. U. Masumdar and M. Sharon, Solar Energy, Vol. 86, 2012, pp. 1910-1919.

[34] Y. C. Lin, J. H. Ke, W. T. Yen, S. C. Liang, C. H. Wu and C. T. Chiang, Appl. Surf. Sci., Vol. 257, 2011, pp. 4278-4284.

[35] M. G. Panthani, V. Akhavan, B. Goodfellow, J. P. Schmidtke, L. Dunn, A. Dodabalapur, P. F. Barbara and B. A. Korgel, J. Am. Chem. Soc., Vol. 130, 2008, pp. 16770-16777.

[36] S. H. Han, F. S. Hasoon, J. W. Pankow, A. M. Hermann and D. H. Levi, Appl. Phys. Lett., Vol. 87, 1005, p. 151904.

[37] M. A. Islam, Q. Huda, M. S. Hossain, M. M. Aliyu, M. R. Karim, K. Sopian and N. Amin, Current Applied Physics, Vol. 13, Suppl. 2, 2013, pp. S115-S121.

[38] A. Bouraiou, M. S. Aida, A. Mosbah and N. Attaf, Brazilian Journal of Physics, Vol. 39, No. 3, 2009, pp. 543-546.

[39] M. L. Fearheiley, K. J. Bachmann, Y. H. Shing, S. A. Vasquez and C. R. Herrington, Journal of Electronic Materials, Vol. 14, No. 6, 1985, pp. 677-683.

[40] A. A. I. Al-Bassam and U. A. Elani, Proceeding of 2012 International Conference on Environment, Energy and Biotechnology, Vol. 33, IACSUT Press, Singapore, 2012, pp. 163-167.

[41] S. Karthikeyan, A. E. Hill, R. D. Pilkington, J. S. Cowpe, J. Hisek and D. M. Bagnall, Thin Solid Films, Vol. 519, 2011, pp. 3107-3112.

[42] H. Khallaf, G. Chai, O. Lupan, L. Chow, S. Park and A. Schulte, Applied Surface Science, Vol. 255, No. 7, 2009, pp. 4129-4134.

[43] D. S. Reddy, K. N. Rao, K. R. Gunasekhar, N. K. Reddy, K. S. Kumar and P. S. Reddy, Materials Research Bulletin, Vol. 43, No. 12, 2008, pp. 3245-3251.

[44] Y. Gu, X. Li, W. Yu, X. Gao, J. Zhao and C. Yang, Journal of Crystal Growth, Vol. 305, No. 1, 2007, pp. 36-39.

[45] S. Wageh, A. A. Higazy and M. A. Algradee, Journal of Modern Physics, Vol. 2, No. 8, 2011, pp. 913-921.

[46] C. V. Ramana, R. J. Smith and O. M. Hussain, Physica Status Solidi A, Vol. 199, No. 1, 2003, pp. R4-R6.

[47] D. Souria and K. Shomalian, J. Non-Cryst. Solids, Vol. 355, 2009, pp. 1597-1601.

[48] J. M. González-Leal, A. Ledesma, A. M. Bernal-Oliva, R. Prieto-Alcón, E. Márquez, J. A. Angel and J. Cárabe, Mater. Lett., Vol. 39, Iss. 4, 1999, pp. 232-239.

[49] S. Chandramohan, R. Sathyamoorthy, P. Sudhagar, D. Kanjilal, D. Kabiraj and K. Asokan, Thin Solid Films, Vol. 516, Iss. 16, 2008, pp.

5508-5512.

[50] R. Sathyamoorthy, Sa. K. Narayandass and D. Mangalaraj, Sol. Energ. Mat. Sol. C., Vol. 76, Iss. 3, 2003, pp. 339-346.

[51] M. S. Oh, D. K. Hwang, D. J. Seong, H. S. Hwang, S. J. Park and E. D. Kim, J. Electrochem. Soc., Vol. 155, No. 9, 2008, pp. D599-D603.

[52] D. H. Cho, K. S. Lee, Y. D. Chung, J. H. Kim, S. J. Park and J. Kim, Appl. Phys. Lett., Vol. 101, 2012, p. 023901.

[53] R. Buonsanti, A. Llordes, S. Aloni, B. A. Helms and Delia J. Milliron, Nano Lett., Vol. 11, 2011, pp. 4706-4710.

[54] H. Neumann and R.D. Tomlinson, Solar Cells, Vol. 28, No. 4, 1990, pp. 301-313.

[55] D. Haneman, Critical Reviews in Solid State and Materials Sciences, Vol. 14, No. 4, 1988, pp. 377-413.

[56] R. Chen and C. Persson, Journal of Applied Physics, Vol. 112, No. 10, 2012, p. 103708.

[57] G. A. Medvedkin and M. A. Magomedov, Semiconductor Science and Technology, Vol. 8, No. 5, 1993, pp. 652-656.

[58] S. R. Kodigala, Cu(In1-xGax)Se2 Based Thin Film Solar Cells, Vol. 35, Academic Press, MA, USA, 2011, p. 215.

[59] A. Knowlcs, H. Oumous. M. J. Carter and R. Hill, Conference Record of the Twentieth IEEE Photovoltaic Specialists Conference, Vol. 2, IEEE, Las Vegas, NV, USA, 1988, p. 1482.

[60] T. Datta, R. Noufi and S. K. Deb, Applied Physics Letters, Vol. 47, No. 10, 1985, pp. 1102-1104.

감사의 글

짧지만 길었던 2년6개월이라는 시간이 다 지나가고, 이제 석사과정을 마칠 시간이 다 되어가고 있습니다. 2011년 처음으로 석사를 하기로 마음먹었던 때, 이렇게 하다 언제 마칠 수 있을지 막연하고 어디서부터 시작해야 할 지 몰라서 당황스러웠습니다. 그렇게 시간이 어느덧 흘러 벌써 석사를 졸업하게 될 시간이 왔습니다. 부족함을 느끼며 아쉬움이 남는 순간 벌써 졸업이라는 시간이 제게 다가왔습니다. 결과야 어떻든 늘 아쉬움이 남지만 좋은 경험을 쌓았으며 좋은 분들을 알게 된 데에 대해서 큰 기쁨을 느낍니다. 아무 탈없이 석사를 졸업하고 졸업논문까지 쓸 수 있도록 도와주신 분들을 위해서 짧게 글로나마 감사의 마음을 전하고 싶습니다.

무엇보다 제게 다시 학업의 기회를 주신 부모님께 감사의 말씀 드립니다. 제가 적지 않은 나이에도 불구하고, 그다지 좋지 않은 상황에도 불구하고, 학업의 길로 나아갈 수 있도록 모든 지원을 해주시고 응원해주신 부모님께 감사를 드립니다. 정말 사랑하고 감사합니다.

기대에 어긋나지 않는 아들이 될 수 있도록 더욱 노력하겠다고 이야기하고 싶습니다. 뿐만 아니라 제 동생 진아에게도 늘 고맙다는 말을 하고 싶었습니다. 제가 고민거리가 있으면 들어주고 동생답지 않은 어른스러움으로 제게 큰 힘이 되어준 내 동생아 사랑한다. 저 먼 나라에서 혼자 고생하고 늘 힘들어 하는 진아에게 힘내라는 말을 하고 싶습니다. 하늘에 계신 저희 할아버지에게도 감사의 말을 전하고 싶습니다. 오랜 투병생활 끝에 올해 초에 우리 곁을 떠나셨는데 좋은 곳에 가서 행복하실 거라고 생각합니다. 사고 이후 말씀은 못하셔도 늘 다정하게 맞아주셔서 감사했었습니다. 눈 오는 날이면 늘 보고 싶습니다.

그리고 부족하고 미흡한 저를 흔쾌히 거둬들여 주시고, 학업적이나 인격적으로 많은 가르침을 주시고 다듬어 주신 이우선 교수님께 큰 감사의 말씀 전합니다. 교수님의 기대만큼 좋은 결과를 내지 못한 부분은 정말 죄송한 마음을 가지고 있습니다. 또한 논문에 대하여 많은 가르침을 주시고 도와주신 김남훈 교수님께 정말 큰 감사를 드리고 싶습니다. 부족한 저에게 기회를 주시고 실험 및 논문작성을 할 수 있도록 물심양면 지원해주신 교수님께 늘 죄송하고 감사한 마음을 가지고 있습니다. 그리고 잘 졸업할 수 있도록 도와주신 조금배 교수님한테도 늘 감사합니다. 이번 석사를 하며 이렇게 도움을 많이 받을 수 있어서 저에게는 큰 복이 아니었나 싶습니다.

그리고 저 석사 기간 내내 졸업할 수 있도록 도와주신 지은씨 정말 미안하고 고맙습니다.

마지막으로 항상 저를 믿고, 응원해주신 세상에서 가장 존경하고 감사드리는 저의 아버지, 한번더 아니 항상 감사합니다.

정동현

저작물 이용 허락서

학 과	전기공학과	학 번	20117445	과 정	석사
성 명	한글 : 정동현 한문 : 鄭東鉉 영문 : Chung Dong Hyun				
주 소	광주광역시 북구 중흥2동 모아아파트 107-1602				
연락처	010-9633-1544	E-mail	donghyeoni@naver.com		
논문제목	한글 : 동시스퍼터링 증착 후 급속열처리 CIS 박막 특성				
	영문 : Characteristics of CIS Thin Films by RTA Process after Co-Sputtering				

본인이 저작한 위의 저작물에 대하여 다음과 같은 조건 아래 - 조선대학교가 저작물을 이용할 수 있도록 허락하고 동의합니다.

- 다 음 -

1. 저작물의 DB구축 및 인터넷을 포함한 정보통신망에의 공개를 위한 저작물의 복제, 기억장치에의 저장, 전송 등을 허락함.
2. 위의 목적을 위하여 필요한 범위 내에서의 편집과 형식상의 변경을 허락함. 다만, 저작물의 내용변경은 금지함.
3. 배포・전송된 저작물의 영리적 목적을 위한 복제, 저장, 전송 등은 금지함.
4. 저작물에 대한 이용기간은 5년으로 하고, 기간종료 3개월 이내에 별도의 의사 표시가 없을 경우에는 저작물의 이용기간을 계속 연장함.
5. 해당 저작물의 저작권을 타인에게 양도하거나 출판을 허락을 하였을 경우에는 1개월 이내에 대학에 이를 통보함.
6. 조선대학교는 저작물 이용의 허락 이후 해당 저작물로 인하여 발생하는 타인에 의한 권리 침해에 대하여 일체의 법적 책임을 지지 않음.
7. 소속 대학의 협정기관에 저작물의 제공 및 인터넷 등 정보통신망을 이용한 저작물의 전송・출력을 허락함.

동의여부 : 동의(○) 반대( )

2014년 2월

저작자: 정 동 현 (인)

조선대학교 총장 귀하